Inorganic Chemistry

pubs.acs.org/IC

Article

Ru(II)-*p*-Cymene Complexes of Furoylthiourea Ligands for Anticancer Applications against Breast Cancer Cells

Dorothy Priyanka Dorairaj, Jebiti Haribabu, Mahendiran Dharmasivam, Rahime Eshaghi Malekshah, Mohamed Kasim Mohamed Subarkhan, Cesar Echeverria, and Ramasamy Karvembu*

Cite This: *Inorg. Chem.* 2023, 62, 11761−11774

Read Online

ACCESS | Metrics & More | Article Recommendations | Supporting Information

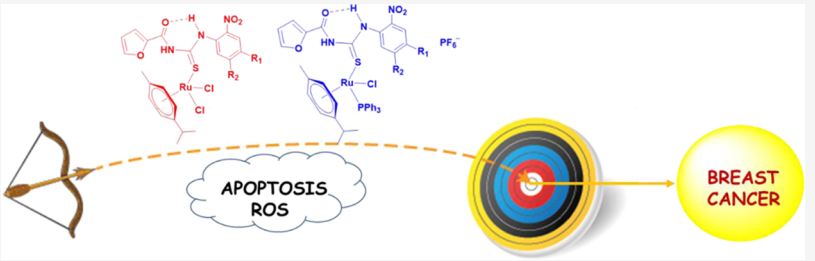

ABSTRACT: Half-sandwich Ru(II) complexes containing nitro-substituted furoylthiourea ligands, bearing the general formula $[(\eta^6\text{-}p\text{-cymene})RuCl_2(L)]$ (**1**−**6**) and $[(\eta^6\text{-}p\text{-cymene})RuCl(L)(PPh_3)]^+$ (**7**−**12**), have been synthesized and characterized. In contrast to the spectroscopic data which revealed monodentate coordination of the ligands to the Ru(II) ion *via* a "S" atom, single crystal X-ray structures revealed an unusual bidentate N, S coordination with the metal center forming a four-membered ring. Interaction studies by absorption, emission, and viscosity measurements revealed intercalation of the Ru(II) complexes with calf thymus (CT) DNA. The complexes showed good interactions with bovine serum albumin (BSA) as well. Further, their cytotoxicity was explored exclusively against breast cancer cells, namely, MCF-7, T47-D, and MDA-MB-231, wherein all of the complexes were found to display more pronounced activity than their ligand counterparts. Complexes **7**−**12** bearing triphenylphosphine displayed significant cytotoxicity, among which complex **12** showed IC_{50} values of 0.6 ± 0.9, 0.1 ± 0.8, and 0.1 ± 0.2 μM against MCF-7, T47-D, and MDA-MB-231 cell lines, respectively. The most active complexes were tested for their mode of cell death through staining assays, which confirmed apoptosis. The upregulation of apoptotic inducing and downregulation of apoptotic suppressing proteins as inferred from the western blot analysis also corroborated the apoptotic mode of cell death. The active complexes effectively generated reactive oxygen species (ROS) in MDA-MB-231 cells as analyzed from the 2′,7′-dichlorofluorescein diacetate (DCFH-DA) staining. Finally, *in vivo* studies of the highly active complexes (**6** and **12**) were performed on the mice model. Histological analyses revealed that treatment with these complexes at high doses of up to 8 mg/kg did not induce any visible damage to the tested organs.

INTRODUCTION

The prevalence of cancer has increased substantially, claiming millions of lives and impacting many across the globe. Based on the American Cancer Society statistics, breast cancer has emerged as the most frequently reported one and also the second highest cause of mortality in women.[1] Despite cisplatin's enormous success as an anticancer drug, its limitations and side effects have forced the scientific community to focus on alternate metallodrugs with minimal side effects and enhanced anticancer efficacy.[2] In the search for developing anticancer agents containing metals other than Pt, Ru complexes have emerged as the most promising ones in recent years. The ligand exchange kinetics for metal complexes in an aqueous medium is one of the crucial factors influencing anticancer activity.[3] Coordination compounds having slow ligand exchange rates, similar to the cell cycle processes, appear to be highly effective in targeting cancer cells. This is especially obvious in Pt and Ru complexes. These metals exhibit almost the same kinetic rate in the order of 10^{-3}−10^{-2} s^{-1}.[4] Organometallic Ru compounds possess remarkable activity against several cancer cell lines. Clarke's group, in 1980, synthesized the first Ru-based classical Werner-type complex $[RuCl_3(NH_3)_3]$, which was tested for its anticancer activity.[5] Thereafter, some polypyridyl complexes of the type *cis*-$[RuCl_2(bpy)_2]$ and *mer*-$[RuCl_3(tpy)]$ were reported by Novakova et al., which exhibited good cytotoxicity on leukemia and colon cancer cells.[6] Importantly, *trans*-[imi-H]-$[RuCl_4(imi)_2]$ and *trans*-[ind-H]$[RuCl_4(ind)_2]$ reported by

Received: March 7, 2023
Published: July 17, 2023

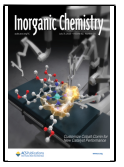

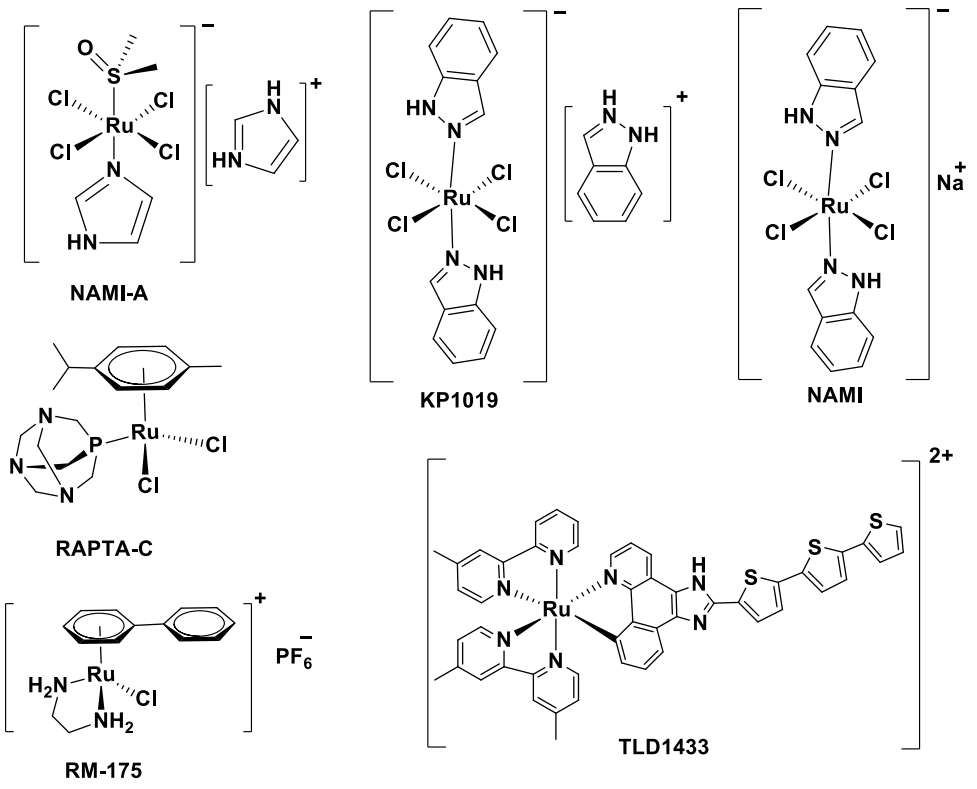

Figure 1. Examples of some well-known Ru(II)/Ru(III) potential anticancer drugs.

Scheme 1. Synthesis of Ligands (L1−L6)

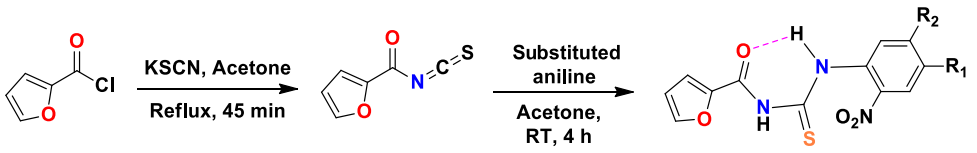

L1 : R_1 = H; R_2 = H
L2 : R_1 = CH_3; R_2 = H
L3 : R_1 = OCH_3; R_2 = H
L4 : R_1 = H; R_2 = Cl
L5 : R_1 = CH_3; R_2 = Cl
L6 : R_1 = CH_3; R_2 = CH_3

Keppler's group exhibited remarkable activity on colorectal cancer cells, which were considered as a breakthrough in the area of Ru complexes as anticancer agents. Further, substantial insights into the anticancer potential of NAMI-A have been reported by Alessio's, Mestroni's, and Sava's groups.[7−12] Ruthenium-based compounds such as NAMI-A, KP1019, KP1339, and TLD1433 had initially entered clinical trials. Owing to less activity and solubility limitations, NAMI-A and KP1019 were dropped out of the trials. Currently, TLD1433 has entered phase IIa human clinical trials (ClinicalTrials.gov, identifier NCT03053635) and has shown to be effective against human non-musculoinvasive bladder cancer.[13−15] Some of the well-known Ru anticancer drugs are illustrated in Figure 1.

The anticancer activity of Ru−arene complexes was first reported by Tocher's group in 1992, wherein the activity of well-known [Ru(η^6-benzene)(metronidazole)Cl_2] was described.[16] Subsequently, Sadler's and Dyson's groups investigated the activity of some Ru−arene complexes.[11,17−19] Recently, Ru(II)−arene complexes containing PPh_3 have been developed, which displayed superior activity against cancer cells.[20−23] The presence of the hydrophobic arene, labile chloride, lipophilic PPh_3, and chelating ligands contribute to their overall anticancer activity. The ligands present in the Ru−arene system are important in controlling anticancer efficacy. One such vital ligand system is aroylthiourea, which has been found to exhibit an array of biological properties.[24] They are air- and moisture-stable and have the ability to exhibit versatile coordination modes with metals due to the presence of O, N, and S donor atoms.[25] Furans are well-known heterocyclic compounds possessing a wide range of therapeutic properties and constitute an important part of natural products such as furanoflavinoids, furanolactones, furanocoumarins, and some terpenoids. In the present work, we report twelve Ru(II)-arene-based furoylthiourea complexes, their interactions with biomolecules, and their cytotoxic properties exclusively against breast cancer cells.

RESULTS AND DISCUSSION

Synthesis of Ligands and Complexes. Refluxing furoyl chloride and potassium thiocyanate in acetone for 1 h, followed by the addition of the corresponding aniline (2-nitroaniline, 4-

https://doi.org/10.1021/acs.inorgchem.3c00757
Inorg. Chem. 2023, 62, 11761−11774

Scheme 2. Synthesis of Complexes (1−6)

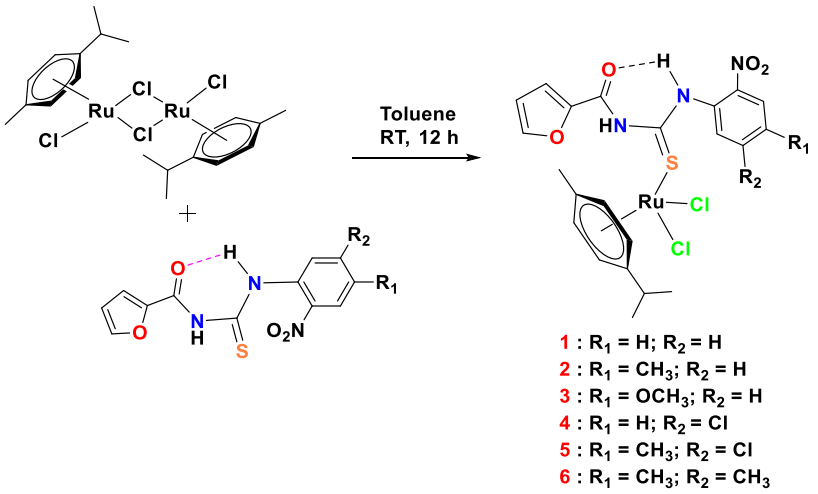

Scheme 3. Synthesis of Complexes Containing PPh_3 (7−12)

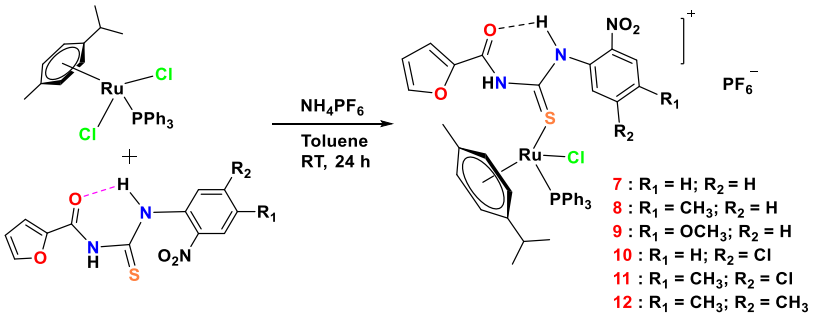

methyl-2-nitroaniline, 4-methoxy-2-nitroaniline, 5-chloro-2-nitroaniline, 5-chloro-4-methyl-2-nitroaniline or 4,5-dimethyl-2-nitroaniline) at room temperature (Scheme 1) resulted in the formation of ligands L1−L6. Among them, ligand L1 was already reported.[26] The treatment of ligands with $[RuCl_2(\eta^6\text{-}p\text{-cymene})]_2$ and $[RuCl_2(\eta^6\text{-}p\text{-cymene})(PPh_3)]$ in 2:1 and 1:1 ratios in toluene for 12 and 24 h, respectively, yielded the corresponding complexes (Schemes 2 and 3).

Spectroscopic Characterization. The ligand and complex formation were confirmed by ultraviolet−visible (UV−vis), Fourier transform infrared (FT-IR), nuclear magnetic resonance (NMR), and electrospray ionization-mass spectrometry (ESI−MS) spectroscopic techniques. The bands appearing in the UV−vis spectra of the ligands at 261−279 and 276−296 nm were characteristic of $\pi \rightarrow \pi^*$ and $n \rightarrow \pi^*$ transitions, respectively.[27] The additional bands seen at 347−365 and 425−459 nm in the spectra of complexes were due to MLCT and d → d transitions, respectively. FT-IR spectra of the ligands exhibited four sharp peaks at 3431−3459, 3081−3189, 1679−1691, and 1248−1269 cm^{-1} that belonged to the amide N−H, thiourea N−H, C═O, and C═S stretching vibrations, respectively. In the spectra of complexes, a noticeable shift (from 1248−1269 to 1171−1186 cm^{-1}) in the stretching frequency of C═S was seen, whereas almost no change in the C═O stretching frequency was observed, indicating the coordination of S to the Ru(II) ion. The stretching frequencies observed at 710−721, 1076−1092, and 1437−1452 cm^{-1} confirmed the presence of PPh_3 in the complexes.[28] FT-IR spectra of the complexes are depicted in Figure S1. ^1H NMR spectra of the ligands showed two singlets at 13.33−12.54 and 11.69−9.30 ppm, which were due to the carbonyl- and thiocarbonyl-attached N−H protons, respectively. Aromatic protons of phenyl and furoyl groups resonated at 6.62−8.67 ppm. In the ^1H NMR spectra of complexes, there was an insignificant change in the signal of the carbonyl-attached N−H proton, whereas the thiocarbonyl-attached N−H proton appeared to be more deshielded compared to that of the ligands, which indicated the coordination of S to the Ru(II) ion. Two sets of doublets at 5.74−5.19 and 5.45−4.98 ppm, a septet at 3.04−2.61 ppm, a singlet at 2.50−1.89 ppm, and a doublet at 1.62−1.08 ppm validated the presence of *p*-cymene in the complexes. The ^{13}C NMR spectra of ligands displayed two signals in the ranges of 179.0−181.1 and 155.9−158.1 ppm, that belonged to thiocarbonyl and carbonyl carbons, respectively, while the aromatic carbons resonated at 109.1−156.2 ppm. The new signals appearing at 109.3−93.5, 100.5−88.9, 91.0−81.2, 89.7−79.7, 30.9−30.3, 22.4−21.2, and 19.7−17.2 ppm in the spectra of complexes verified the existence of *p*-cymene.[29] In addition, 2D NMR techniques such as $^1H-^{13}C$ HSQC and NOESY for representative ligand (L1) and complex (**1**) were employed to better understand the proton and carbon interactions. The appearance of a singlet in the ^{31}P NMR spectra at 29.43−31.87 ppm proved the coordination of PPh_3 to Ru, while a septet found in the region −146.5 to −135.5 ppm in the case of complexes **7**−**12** was due to PF_6.[30] ^{31}P NMR chemical shift values for complexes **7**−**12** are listed in Table S1. The NMR spectra for L1−L6 and **1**-−**12** are depicted in Figures S2−S43. The 2D NMR spectra for L1 and complex **1** are shown in Figures S44−S47. ESI−MS spectra of complexes **1**−**6** displayed an *m*/*z* value corresponding to $[M - HCl - Cl^-]^+$,

https://doi.org/10.1021/acs.inorgchem.3c00757
Inorg. Chem. 2023, 62, 11761−11774

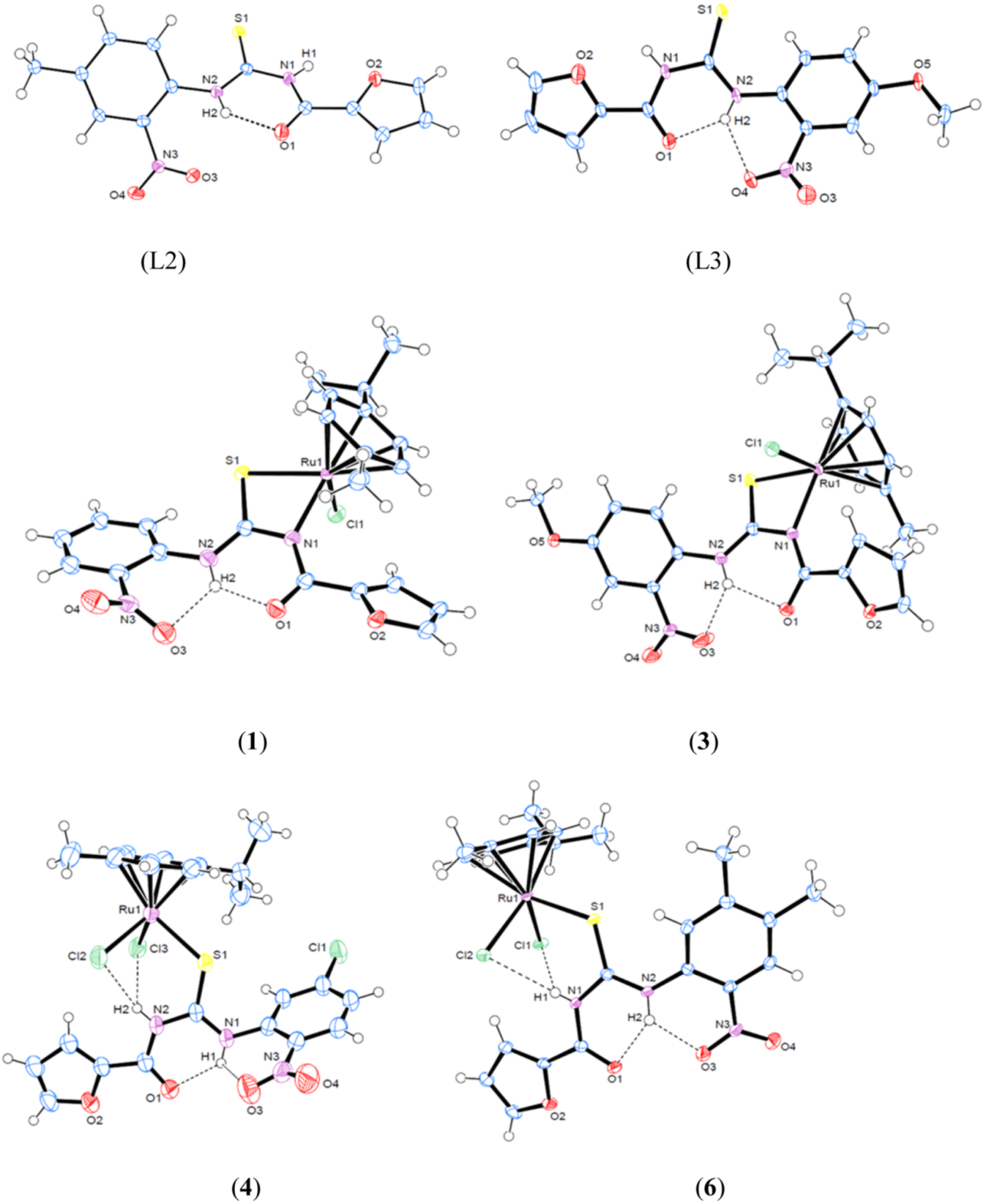

Figure 2. X-ray structures of L2, L3, **1**, **3**, **4**, and **6**.

while complexes **7**−**12** displayed a molecular ion peak due to $[M - PF_6^-]^+$ (Figures S48−S59).

Solid-State Structures. Single crystals of the ligands were obtained by slow evaporation of their acetonitrile solutions, while crystals of the complexes were obtained by evaporation of their DMF-dichloromethane (2:98) solutions. In contrast to the results obtained from spectroscopy, an unusual bidentate coordination of the furoylthiourea ligands through N, S atoms

https://doi.org/10.1021/acs.inorgchem.3c00757
Inorg. Chem. 2023, 62, 11761−11774

with the Ru(II) ion was seen in complexes **1** and **3**, whereas the monodentate coordination involving only S was observed in complexes **4** and **6**. Such N, S coordination of aroylthiourea ligands with Ru(II)-arene in the solid state has already been reported by Cunha, Parveen, Obradović, and Swaminathan et al.[21,31−33] Figure 2 illustrates the thermal ellipsoid plots for the ligands and complexes, as well as the atomic labeling schemes. Crystal data and selected bond lengths and angles for the ligands and complexes are summarized in Tables S2−S5. Ligands L2 and L3 crystallized in a monoclinic fashion with the *P21/c* space group. Complexes **1** and **3** adopted a *pseudo*-tetrahedral piano-stool geometry encompassing N, S-coordinated aroylthiourea, *p*-cymene, and chlorido ligands. In the complexes, an intramolecular hydrogen bonding was observed between the thioamide N−H and carbonyl oxygen. Also, an intramolecular hydrogen bonding between amide N−H, carbonyl oxygen, and NO_2 was observed in the crystal pattern of complexes **1**, **3**, **4**, and **6**. In addition, a hydrogen-bonding interaction was observed between the amide N−H and one of the chlorido ligands. The Ru−C bond lengths were in the region 2.152−2.233 Å, while the Ru−S, Ru−Cl, and Ru−N bond distances were in the ranges of 2.326−2.360, 2.378−2.396, and 2.254−2.274 Å, respectively, which were in line with the literature values.[34,35]

Interaction with Biomolecules. *Complex−CT DNA Interaction.* Figure S60 depicts the absorption spectra of the Ru(II) complexes with and without CT DNA. The addition of CT DNA to the Ru(II) complexes led to a decrease in absorbance, creating a hypochromic effect accompanied by a small red shift (2−5 nm). Compounds exhibiting noncovalent interactions with DNA generally display hypochromism owing to the stacking interactions between the aromatic chromophore and the DNA base pairs. The extent of binding was understood from the intrinsic binding constant (K_b) values deduced from the Wolfe−Shimmer equation.[36] The plots of [DNA]/($\varepsilon_a - \varepsilon_f$) *versus* [DNA] are shown in Figure S61, and the K_b values are listed in Table S6. The complexes holding PPh_3 (**7**−**12**) displayed better binding than complexes **1**−**6**. This could be linked to the presence of phenyl rings (of PPh_3), resulting in enhanced planarity and $\pi-\pi$ aromatic stacking interactions with the DNA base pairs.[37] Among the different substituents, the complexes bearing an electron-donating substituent (methyl or methoxy) exhibited the highest binding ability with DNA, which agreed with the literature.[38]

As the Ru(II) complexes remained nonfluorescent, their binding with CT DNA could not be directly predicted from emission studies. Hence, competitive binding with ethidium bromide (EB) was performed. Figure S62 depicts the emission spectra of the EB−DNA mixture in the absence and presence of the complexes wherein a decrease in the fluorescence intensity at 610 nm was observed upon the addition of Ru(II) complexes (0−50 μM) to EB−DNA. The slope of the plot of F^o/F *versus* [Q] gave K_q (Figure S63). The extent of quenching (K_q) was calculated from the Stern−Volmer equation.[39] The K_q and K_{app} values are listed in Table S6. Viscosity studies were carried out to understand the nature of binding interactions. This hydrodynamic experiment is sensitive to changes in the DNA chain length, and binding interactions such as covalent and noncovalent can be distinguished based on the changes in viscosity levels.[40] Intercalators generally tend to slide in between the DNA base pairs, leading to elongation of the helical strand, resulting in increased viscosity. In the case of noncovalent major and minor groove binding, negligible changes in viscosity are seen. In contrast, the covalent binding interactions result in a decrease in viscosity as covalent binders bind to the sides of the DNA helix that results in a breakage/kinking of the helical strand. The changes in the viscosity of CT DNA upon the incremental addition of Ru(II) complexes are depicted in Figure S64. EB was used as a positive control while $[Co(NH_3)_6]Cl_3$ was chosen as a negative control.[41] An increase in viscosity was seen with the addition of complexes **1**−**12** to CT DNA, suggesting intercalation. However, the effect of intercalation was less when compared to EB, and greater when compared to $[Co(NH_3)_6]$-Cl_3.

Complex−BSA Interaction. To understand the complex−protein interaction, a binding study with BSA was performed. An enhancement in absorbance was seen upon the addition of the complexes at 280 nm, which indicated the static nature of binding between BSA and complexes (Figure S65).[42] Further, the interaction between the complexes and BSA was studied through fluorescence spectroscopy. The fluorescence spectra were recorded in the range of 290−500 nm upon excitation at 280 nm. An incremental addition of the Ru(II) complexes (0−18 μM) to BSA (1 μM) resulted in the quenching of fluorescence at 345 nm, which was accompanied by a minor hypsochromic shift (Figure S66). This quenching was due to the active sites of the protein being buried inside a hydrophobic pocket.[43] In addition, the inner filter effect of the Ru(II) complexes was corrected using the equation, $F_{corr} = F_{obs} \times e^{(A_{ex}+A_{em})/2}$, where F_{corr} is the corrected fluorescence intensity, F_{obs} is the observed intensity, and A_{ex} and A_{em} are the absorbances of the compounds at excitation and emission wavelengths, respectively.[44] From the Stern−Volmer equation, the plot of F^o/F *versus* [Q] was deduced as shown in Figure S67. By employing the Scatchard equation, the plot of log [(F^o-F)/F] *versus* log[Q] was deduced (Figure S68), from which the number of binding sites (n) and binding constant (K_b) values were obtained. The values of K_b, K_q, and n are listed in Table S7.

Docking of the Ru(II) Complexes with Biomolecules (DNA and BSA). The interactions of DNA and BSA with the Ru(II)−arene complexes were further visualized by molecular docking studies using Molegro software with the chosen targets DNA (PDB ID: 1Z3F) and BSA (PDB ID: 3V03). From the docked images of complexes (Figure S69), we could infer that the complexes, by and large, got inserted between the DNA helical strands, confirming intercalation on par with the results obtained from absorption and emission spectral studies. Complexes **7**−**12** containing PPh_3 exhibited better docking energy scores than complexes **1**−**6**, which could be due to the enhanced stacking interactions between the phenyl rings and DNA base pairs. Based on the docking energy scores (Table S8), the complexes showed good interaction with BSA as well (Figure S70).

Lipophilicity Measurements. Lipophilicity is a key pharmacodynamic and pharmacokinetic characteristic that impacts drug absorption, metabolism, distribution, excretion, and toxicity (ADMET). The partition coefficient, Log *P*, which can be defined as the propensity of a neutral (uncharged) compound to dissolve in an immiscible biphasic system of lipid (fats, oils, or organic solvents) and water or in simple terms, the ratio of partitioning between octanol and water, can be used to describe a drug's lipophilicity.[45] A negative Log *P* value indicates that the compound has a higher affinity for the aqueous phase (it is more hydrophilic); when Log *P* = 0, the compound is equally partitioned between the lipid and aqueous phases; and a positive Log *P* value indicates that the compound has a higher concentration in the lipid phase (it is more lipophilic). Log *P* = 1 indicates a 10:1 partitioning in the organic−aqueous phases.

https://doi.org/10.1021/acs.inorgchem.3c00757
Inorg. Chem. 2023, 62, 11761−11774

Table 1. IC_{50} (μM) Values and Selectivity Index (S.I) of the Ru(II) Complexes and Cisplatin after 72 h Incubation at 37 °C

	IC_{50} (μM)				S.I		
compound	MCF-7	T47-D	MDA-MB-231	MCF-10a	MCF-7	T47-D	MDA-MB-231
L1	39.2 ± 0.5	36.4 ± 0.6	36.8 ± 0.8	>50	1.27	1.37	1.35
L2	29.5 ± 0.1	26.8 ± 0.8	27.1 ± 0.5	>50	1.69	1.86	1.84
L3	27.6 ± 0.9	23.6 ± 0.5	24.4 ± 0.5	>50	1.81	2.11	2.04
L4	43.0 ± 0.5	39.7 ± 1.0	40.2 ± 0.7	>50	1.16	1.25	1.24
L5	34.4 ± 0.2	30.1 ± 0.8	31.2 ± 0.6	>50	1.45	1.66	1.60
L6	25.3 ± 0.1	23.5 ± 0.3	23.9 ± 1.0	>50	1.97	2.12	2.09
1	19.3 ± 0.6	16.2 ± 0.4	16.7 ± 0.4	>50	2.59	3.08	2.99
2	13.6 ± 0.8	11.4 ± 0.2	11.4 ± 1.2	>50	3.67	4.38	4.38
3	12.5 ± 0.5	10.0 ± 0.8	10.3 ± 0.3	>50	4.00	5.00	4.85
4	28.6 ± 0.3	24.2 ± 0.9	21.6 ± 0.4	>50	1.74	2.06	2.31
5	14.6 ± 0.3	12.1 ± 0.2	12.9 ± 0.9	>50	3.42	4.13	3.87
6	9.8 ± 0.2	8.5 ± 0.4	8.6 ± 0.6	>50	5.10	5.88	5.81
7	2.4 ± 0.1	1.2 ± 0.9	1.2 ± 0.4	>50	20.83	41.66	41.66
8	1.5 ± 0.8	0.4 ± 0.6	0.5 ± 0.5	>50	33.33	125.00	100.00
9	1.1 ± 0.6	0.1 ± 0.8	0.1 ± 0.2	>50	45.45	500.00	500.00
10	3.9 ± 0.5	2.8 ± 0.7	2.8 ± 1.2	>50	12.82	17.85	17.85
11	1.6 ± 0.7	0.9 ± 0.5	0.8 ± 0.3	>50	31.25	55.55	62.5
12	0.6 ± 0.9	0.1 ± 1.0	0.1 ± 0.2	>50	83.33	500.00	500.00
cisplatin	19.4 ± 0.5	15.8 ± 0.1	7.1 ± 0.8	28.7 ± 0.8	1.47	1.81	4.04

High lipophilicity (Log P > 5) often contributes to high metabolic turnover, low solubility, and poor oral absorption, thereby hampering the drug's bioavailability. Compounds with a Log P index higher than 1 or less than 4 are considered to have good physicochemical properties suitable for oral consumption. In the present work, the Log P values of complexes (**1**−**12**) were determined by the shake flask procedure. Figure S71 depicts the lipophilicity diagram of the Ru(II) complexes, while Table S9 depicts their Log P values. All of the complexes showed a Log P value in the range of 1.2−3.1. Compared to the dichlorido complexes, complexes **7**−**12** bearing PPh_3 had a slightly greater lipophilicity index.

Solution Behavior of the Complexes. The hydrolysis process is widely thought to be a crucial activation step inside the cell before the drug reaches the intracellular DNA target. It has been well documented in the literature that for the $[Ru(\eta^6\text{-arene})Cl(en)]^+$ (arene = *p*-cymene, benzene or dihydroanthracene) systems, the hydrolysis of Ru−Cl bond to form $[Ru(\eta^6\text{-arene})(H_2O)(en)]^+$ aqua species may activate the complex for DNA binding.[46] In the present case, the stability assessment of the complexes in 1:99 (v/v) DMSO−water medium through absorption spectroscopy for 72 h ensured that all of the complexes were stable with no alteration or formation of new bands (Figure S72). Then, the hydrolysis of active complexes **6** and **12** in the presence of chloride ions (4 mM and 100 mM NaCl) was studied. Almost no suppression of hydrolysis was seen at a 4 mM concentration of NaCl, but the extent of hydrolysis was considerably suppressed at 100 mM NaCl (Figure S73). These results positively indicated that the complexes were capable of surviving in bloodstream conditions where a high concentration of chloride ions is present.[46]

To evaluate the kinetics of hydrolysis, time-dependent absorption spectra for the complexes were recorded in 100 mM $NaClO_4$ solution, from which the plot of ΔA *versus* K was obtained (Figure S74), where $\Delta A = \Delta_t - \Delta_o$ (Δ_t = absorbance at time t ; Δ_o = absorbance at t = 0.2 min). The presence of isobestic points as seen from the spectra implied that an equilibrium existed between the aqua and chlorido/PPh_3 complexes, and this equilibrium was attained in 1 h (Figure S75). The isobestic points observed around 325 and 350 nm were chosen for monitoring the kinetics for half an hour. The plots of absorbance *versus* time are depicted in Figure S76. By performing a nonlinear regression analysis using Origin 8.5 pro software, it was understood that the complexes (**1**−**12**) obeyed a *pseudo*-first-order kinetics. The corresponding rate constants (K_{obs}) and half-life time ($t_{1/2}$) were calculated from the formulae $k = 1/t$ and $t_{1/2} = 0.693/k$. From the calculated values (Table S10), it is inferred that complexes **6** and **12** displayed the highest rate constants and shortest half-life. The relative K_{obs} and $t_{1/2}$ order of the complexes was **6** > **3** > **5** > **1** > **4** (complexes bearing two chlorido ligands) and **12** > **9** > **8** > **11** > **7** > **10** (complexes bearing one PPh_3 and one chlorido ligands). The inclusion of electron-donating group(s) in the phenyl rings might result in an increase in electron density around the Ru(II) ion, which might have increased the lability of chlorido and PPh_3, thereby facilitating hydrolysis. Hence, the complexes with electron-donating group(s) such as methyl and methoxy exhibited a higher rate of hydrolysis than the ones with electron-withdrawing group(s).

In Vitro Cytotoxicity of the Ru(II) Complexes. Based on the binding interactions with DNA and BSA, we further explored the cytotoxicity of Ru(II) complexes against breast cancer cells, namely, MCF-7, MDA-MB-231, and T47-D. To ensure their selectivity, the activity on a normal MCF-10a cell line was evaluated. From the MTT assay results, we observed that, surprisingly, both the ligands and their Ru(II) complexes displayed remarkable cytotoxicity against the three breast cancer cell lines in a dose-dependent manner. The IC_{50} values of ligands ranged 27.65−43.08, 23.52−39.71, and 23.98−40.82 μM against MCF-7, MDA-MB-231, and T47-D cancer cells, respectively, after 72 h of incubation. The complexes portrayed much higher cytotoxicity than their ligands, highlighting the role of Ru(II) ion and arene moiety. Compared to complexes **1**−**6** which contain two labile chlorido ligands, complexes **7**−**12** containing one chlorido and one PPh_3 exhibited greater cytotoxicity portraying IC_{50} values of 0.62−3.98, 0.15−2.81, and 0.17−2.88 μM against MCF-7, MDA-MB-231, and T47-D cell lines, respectively. It was concluded that the presence of

https://doi.org/10.1021/acs.inorgchem.3c00757
Inorg. Chem. 2023, 62, 11761−11774

Table 2. Anticancer Activity of the Reported Ru(II)−Arene Aroylthiourea Complexes against Breast Cancer Cells

literature	MCF-7	MDA-MB-231	MCF-10a
Rohini et al.[48]	15.2−48.0 ± 0.5 μM		
Rohini et al.[34]	53.0 and 98.1 ± 0.5 μM		
Cunha et al.[22]		0.2−0.7 ± 0.5 μM	3.14−6.67 ± 0.95 μM
Oliveira et al.[23]		0.1−0.2 ± 0.5 μM	0.5−0.7 ± 0.5 μM
Barolli et al.[49]	8.9 and 12.2 μM		
Becceneri et al.[50]		9.3−21.9 ± 0.5 μM	7.9−29.4 ± 0.5 μM
Colina-Vegas et al.[51]			9.3−31.0 ± 0.5 μM
Jeyalakshmi et al.[52]	52.3 → 500 μM		
Jeyalakshmi et al.[53]	151.2−162.9 ± 0.5 μM		
Becceneri et al.[54]		33.4 μM	
this work	0.6−3.9 μM	0.1−2.8 μM	>50 μM

lipophilic PPh_3 and electron-donating substituents such as methyl and methoxy enhanced the activity of complexes.[47] Complexes **6** and **12** bearing two methyl groups exhibited the highest anticancer activity against MDA-MB-231 cancer cell line. Notably, the cytotoxicity of the complexes was much greater than cisplatin, and positively, they exhibited less toxicity on the normal MCF-10a cell line. The IC_{50} values of the ligands and complexes along with their selectivity index are shown in Table 1. The selectivity index (S.I) was calculated by using the formula IC_{50} of MCF-10a/IC_{50} of the cancer cells. Compared to the literature results, the synthesized Ru(II)−arene complexes displayed superior activity toward the breast cancer cells (Table 2).

Validation of Apoptosis. Based on the encouraging results obtained from the MTT assay, we investigated the mode of cell death in the MDA-MB-231 cancer cell line upon treatment with complexes **2**, **3**, **6**, **8**, **9**, **11**, and **12** at 20 μM concentration. From the color transformation visualized in AO/EB staining and nuclear fragmentation pattern observed in DAPI staining, the mode of cell death could be predicted. In AO/EB staining, live cells emit green fluorescence while early apoptotic cells display yellow fluorescence; late apoptotic cells exhibit orange fluorescence, and necrotic cells give out red fluorescence.[55] As shown in Figure 3, yellow fluorescence exhibited by complexes

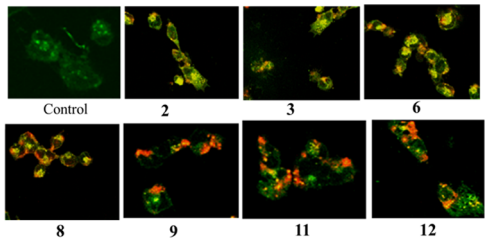

Figure 3. MDA-MB-231 cancer cells stained with AO/EB after being treated with the active complexes at a concentration of 25 μM.

2, **3**, and **6** indicated that these complexes induced early apoptosis in MDA-MB-231 cells. Complexes **8**, **9**, **11**, and **12** bearing PPh_3 emitted bright orange fluorescence, which revealed that these complexes induced late apoptosis in the MDA-MB-231 cancer cell line. To visualize the nuclear alterations taking place in MDA-MB-231 cells, DAPI staining was employed. DAPI is a cell-permeable, fluorescent dye that predominantly binds to the adenine-thymine regions of DNA. Upon detection of apoptosis, the dye emits a bright blue fluorescence at 457 nm.[56] From the confocal microscopic images (Figure 4), we could see that compared to the control cells that exhibited no

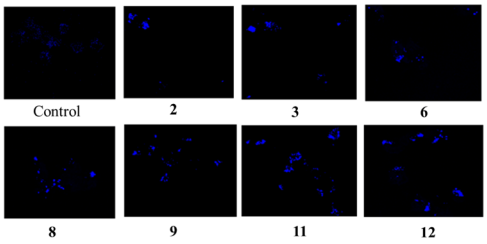

Figure 4. MDA-MB-231 cancer cells stained with DAPI after being treated with the active complexes at a concentration of 25 μM.

fluorescence, blue fluorescence was seen in MDA-MB-231 cells upon treatment with complexes **2**, **3**, and **6** (20 μM), indicating that these complexes were capable of inducing apoptosis. On the other hand, bright fluorescent fetches in MDA-MB-231 cells treated with complexes **8**, **9**, **11**, and **12** (20 μM) were observed, indicating that PPh_3 complexes were able to promote apoptosis in a much better way than the former ones.

Intracellular ROS Generation. Mitochondria, "powerhouse of the cells", is the primary site for intracellular reactive oxygen species (ROS) production. Although optimum levels of ROS can be beneficial, excessive accumulation can promote cancer due to oxidative stress and cellular dysfunction in the cell.[57] A characteristic trait that distinguishes a cancer cell from a normal cell is its ability to generate excess ROS and its increased dependence on an antioxidant defense system.[58] Here, the ROS levels were detected using the DCFH-DA staining assay. Upon entering the cells, DCFH-DA undergoes deacetylation to form DCFH which is nonfluorescent in nature. Further, upon oxidation by ROS, dichlorodihydrofluorescein (DCFH) gets converted to dichlorofluorescein (DCF), which emits bright green fluorescence at 520 nm upon excitation at 495 nm.[59] The images depict ROS generation in MDA-MB-231 cells on treatment with active complexes **2**, **3**, **6**, **8**, **9**, **11**, and **12** at 20 μM concentration (Figure 5). No fluorescence was seen in the control cells, but a considerable extent of green fluorescence was emitted by MDA-MB-231 cells treated with complexes **2**, **3**, and **6**. However, intense green fluorescence fetches were seen with complexes **8**, **9**, **11**, and **12**, indicating that PPh_3 complexes had a greater ability to generate ROS in the cancer cell line, thereby promoting apoptosis.[60] The enhanced ability of PPh_3-bearing complexes (**8**, **9**, **11**, and **12**) to generate excess ROS could be attributed to the charge of these complexes and mitochondria. Since this organelle is negatively charged, positively charged cations could easily permeate through the mitochondrial membrane, leading to better drug absorption.[61] Since complexes **7**−**12** contain an overall positive charge in contrast to complexes

https://doi.org/10.1021/acs.inorgchem.3c00757
Inorg. Chem. 2023, 62, 11761−11774

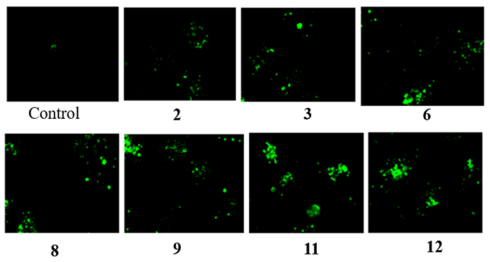

Figure 5. MDA-MB-231 cells stained with DCFH-DA upon treatment with the active complexes at 25 μM.

1−**6** which are neutral, they could permeate easily across the mitochondrial membrane.[62] Parallelly, 2′,7′-dichlorodihydrofluorescein diacetate (H_2DCFH-DA) is said to be negatively charged due to the presence of two acetyl units (CH_3COO^-), which could make these complexes interact strongly with this dye, leading to an excess generation of ROS in MDA-MB-231 cancer cells.

Flow Cytometry Analysis. Flow cytometry analysis for the most active complexes (**6** and **12**) on MDA-MB-231 cells was carried out to analyze the cell count at each stage of the cell cycle. Upon treatment with different concentrations of complexes **6** and **12** (10, 25, and 50 μM), the corresponding change in the cell count at the G0/G1, S, and G2/M phases was seen after 48 h (Figure 6a). The control cells showed a percentage count of 59.78, 15.84, and 19.91 in the G0/G1, S, and G2/M phases, respectively. Complex **6** displayed 47.51 (G0/G1), 12.18 (S), and 17.79% (G2/M), while complex **12** exhibited a count of 40.95 (G0/G1), 8.71 (S), and 10.78% (G2/M). Based on the change in the cell count at the three stages of the cell cycle, it was concluded that both the complexes induced the cell cycle arrest in MDA- MB-231 cells at the G0/G1 phase. The percentage of cells at the three phases is listed in Table 3.

Intrinsic Mediated Apoptosis Pathway. Lastly, western blotting was performed to understand the occurrence of apoptosis in MDA-MB-231 cells by measuring the levels of apoptotic markers such as caspase-3, caspase-9, Bcl-2, and Bax. The Bcl-2 protein, situated in the outer mitochondrial region, is known to control the intrinsic apoptosis pathway by suppressing apoptosis.[63] Caspase-3 and caspase-9 proteins are members of the aspartate-specific cysteine proteases that are known to promote apoptosis. The Bax is a nuclear-encoded protein located in the outer mitochondrial membrane, which is said to be anti-apoptotic.[64] From Figure 7, an overexpression of caspase-3 and caspase-9 proteins and a downregulation of Bcl-2 and Bax proteins in the cancer cell line were observed. The expression of these apoptotic markers inferred that both the active complexes (**6** and **12**) promoted apoptosis.

Table 3. Percentage of Cells at the G0/G1, S and G2/M Phases

compound	G0/G1	S	G2/M
control	59.78 ± 0.76	15.84 ± 0.29	19.91 ± 0.31
6	47.51 ± 1.05	12.18 ± 0.48	17.79 ± 0.92
12	40.95 ± 0.11	8.71 ± 0.36	10.83 ± 1.08

***In Vivo* Study.** As complexes **6** and **12** emerged as the most active ones as inferred from *in vitro* experiments, their *in vivo* potential in the healthy ICR models was analyzed. The mice (n = 8, four females and four males in each group) were intraperitoneally injected with complexes **6** or **12** (2, 4, 6, 8, and 16 mg/kg in DMSO) 5 times on alternate days. The animal models were also administered with controls such as DMSO and saline for a comparative study. Upon visualization of the results, it was inferred that all of the mice treated with cisplatin (4 mg/kg) did not survive, whereas the mice administered with complexes **6** and **12** with dosages of 8 and 16 mg/kg exhibited survival rates of 100 and 80%, and 100 and 74%, respectively. Further, hematoxylin and eosin staining analyses were performed for complexes **6** (8 mg/kg), **12** (8 mg/kg), and cisplatin (4 mg/kg) to analyze the morphological alterations in kidneys, lungs, spleen, liver, and heart. Figure 8 picturizes the microscopic images of the organ tissues, which revealed that the organs, especially lungs, heart, and kidneys administered with complexes **6** and **12**, displayed the normal presence of the glomerular capsules, cytoplasm, alveolar sacs, cardiac muscle fibers, and tubular epithelial cells. On the contrary, photomicrographs of the organs treated with cisplatin showed severe inflammation and edema of the kidneys, degeneration of the distal and proximal epithelial cells, accumulation of vesicles in the cytoplasm, and damage to the alveolar sacs. From these histological images, it is evident that the administration of Ru(II) complexes **6** and **12** in the mice models did not cause any obvious damage to the organ tissues.[33]

CONCLUSIONS

Furoylthiourea ligands and their Ru(II)-*p*-cymene complexes (**1**−**12**) were synthesized and characterized by spectroscopic methods. Although all of the complexes (**1**−**12**) displayed a

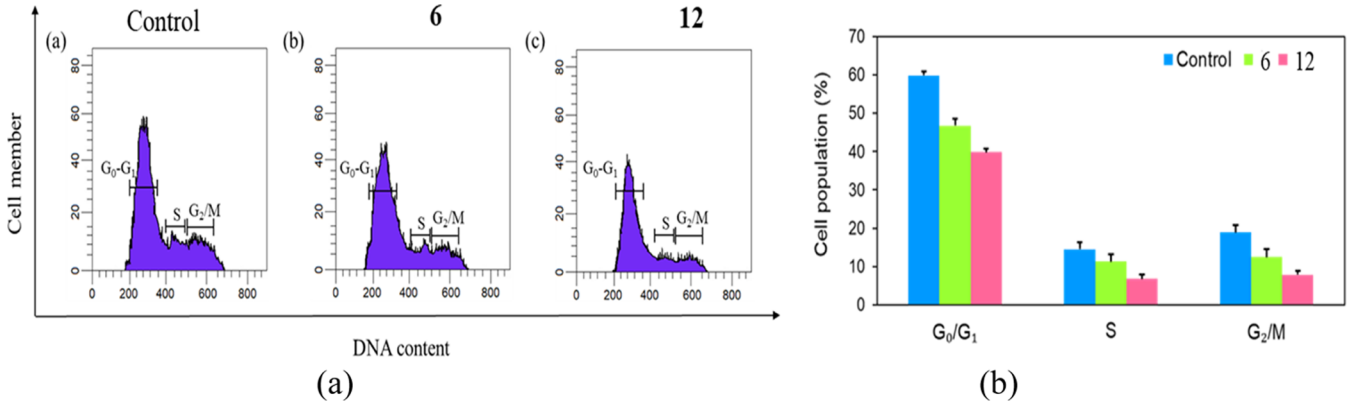

Figure 6. (a) Cell cycle arrest in MDA-MB-231 cells with control, complex **6**, and complex **12** and (b) percentage cell count at each phase of the cell cycle.

https://doi.org/10.1021/acs.inorgchem.3c00757
Inorg. Chem. 2023, 62, 11761−11774

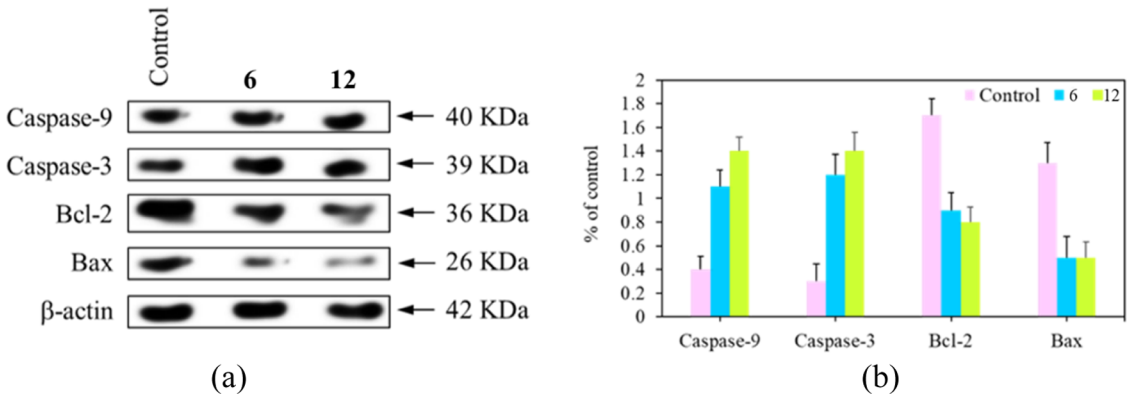

Figure 7. (a) Expression levels of pro- and anti-apoptotic proteins in MDA-MB-231 cancer cell line upon treatment with complexes **6** and **12** and (b) the percentage expression of protein levels in the cancer cell treated with complexes **6** and **12** for 48 h.

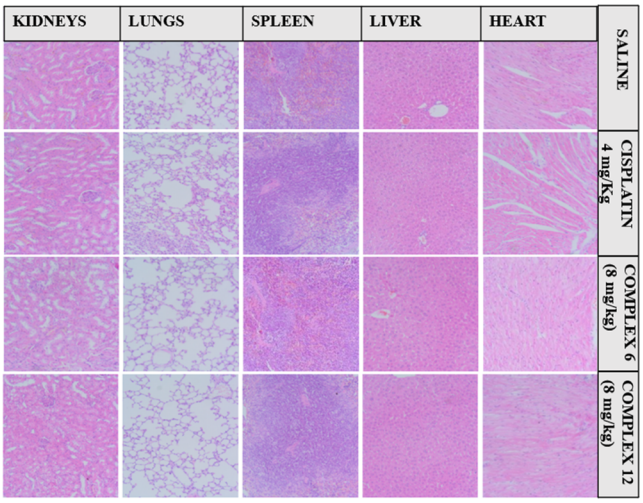

Figure 8. Mice organs (kidneys, lungs, spleen, liver, and heart) treated with saline, cisplatin (4 mg/kg), complex **6** (8 mg/kg), and complex **12** (8 mg/kg) were stained with hematoxylin and eosin.

monodentate coordination of the furoylthiourea ligands with the Ru(II) ion *via* S in their solution state, X-ray structures of complexes **1** and **3** revealed a bidentate N, S coordination of the ligands with the Ru(II) ion, and those of **4** and **6** showed a monodentate coordination of the ligands. Further, biomolecular (DNA and BSA) interaction studies (absorption, emission, and docking) with the complexes revealed that complexes of the type $[(\eta^6\text{-}p\text{-cymene})\mathrm{RuCl(L)(PPh_3)}]^+$ (**7**−**12**) displayed greater binding affinity than $[(\eta^6\text{-}p\text{-cymene})\mathrm{RuCl_2(L)}]$ (**1**−**6**). Noncovalent binding interactions (intercalation) of the complexes with CT DNA were inferred from the spectroscopic analysis. Thereafter, *in vitro* cytotoxicity against breast cancer cells, namely, MCF-7, T47-D, and MDA-MB-231, and a normal cell line (MCF-10a) was evaluated. The IC_{50} values revealed that the complexes possessed greater activity than their ligand counterparts. Positively, they remained noncytotoxic on the normal MCF-10a cell line. Complexes **6** and **12** emerged as the most active ones, displaying remarkable IC_{50} values against the MDA-MB-231 cancer cell line (8.5 and 0.1 μM). Further, these two complexes induced apoptosis on the above cancer cell line, which was inferred from AO/EB staining, DAPI staining, western blot, and flow cytometry analyses. Lastly, *in vivo* results indicated that these two complexes did not cause any noticeable damage to the organs of the mice. The findings obtained from this work conclude that half-sandwich Ru(II)−arene aroylthiourea complexes continue to serve as potential anticancer agents and in future, their anticancer activity could be further enhanced by tuning the mode of coordination, the choice of terminal substituents, and the presence of other biologically important heterocycles apart from furan.

EXPERIMENTAL SECTION

Furoylthiourea Ligand Synthesis. Ligands L1−L6 were synthesized according to literature procedures.[65,66] In a 500 mL round-bottom flask, furoyl chloride (1.984 g, 10 mmol) and potassium thiocyanate (0.971 g, 10 mmol) were taken in acetone and refluxed for an hour. After cooling the reaction mixture, the corresponding aniline (0.841−1.229 g, 10 mmol) was added, and the mixture was stirred for 4 h. The progress of the reaction was monitored by thin-layer chromatography. On completion, HCl (0.1 N, 500 mL) and distilled water (500 mL) were added to the mixture, which led to the formation of a yellow precipitate, which was washed well with water and dried *in vacuo*.

***N*-((2-nitrophenyl)carbamothioyl)furan-2-carboxamide (L1).** Yield: 82%. Light yellow solid. Mp: 162 °C. Anal. Calcd. for $C_{12}H_9N_3O_4S$ (%): C, 49.48; H, 3.11; N, 14.43; S, 11.01. Found: C, 49.51; H, 3.15; N, 14.46; S, 11.05. UV−vis (CH_3CN): λ_{max}, nm (ε, dm^3 mol^{-1} cm^{-1}) 271 (7535), 292 (9939). FT-IR (KBr, cm^{-1}): 3431 (m; ν(amide N−H)), 3081 (s; ν(thioamide N−H)), 1682 (s; ν(C═O)), 1264 (s; ν(C═S)). ^{1}H NMR (400 MHz, $CDCl_3$): δ, ppm 13.18 (s, 1H, O═CNH), 9.35 (s, 1H, S═CNH), 8.48 (d, J = 9.3 Hz, 1H, phenyl), 8.12 (d, J = 8.3 Hz, 1H, phenyl), 7.67 (dd, J = 16.4, 7.9 Hz, 2H, furoyl), 7.49−7.37 (m, 2H, phenyl), 6.66 (dd, J = 3.6, 1.7 Hz, 1H, furoyl). ^{13}C NMR (100 MHz, $CDCl_3$): δ, ppm 179.0 (C═S), 156.3 (C═O), 146.6 (furoyl), 144.9 (O_2N−C), 142.3 (furoyl), 133.4, 132.3, 128.2, 126.8, 125.1 (phenyl), 119.7, 113.8 (furoyl).

***N*-((4-methyl-2-nitrophenyl)carbamothioyl)furan-2-carboxamide (L2).** Yield: 78%. Bright yellow solid. Mp: 164 °C. Anal. Calcd. for $C_{13}H_{11}N_3O_4S$ (%): C, 51.14; H, 3.63; N, 13.76; S, 10.50. Found: C, 51.10; H, 3.60; N, 13.72; S, 10.48. UV−vis (CH_3CN): λ_{max}, nm (ε, dm^3 mol^{-1} cm^{-1}) 274 (7539), 296 (9942). FT-IR (KBr, cm^{-1}): 3449 (m; ν(amide N−H)), 3094 (s; ν(thioamide N−H)), 1690 (s; ν(C═O)), 1256 (s; ν(C═S)). ^{1}H NMR (400 MHz, $CDCl_3$): δ, ppm 13.03 (s, 1H, O═CNH), 9.30 (s, 1H, S═CNH), 8.27 (d, J = 8.4 Hz, 1H, phenyl), 7.90 (d, J = 1.5 Hz, 1H, furoyl), 7.61 (d, J = 1.4 Hz, 1H, furoyl),7.50−7.33 (m, 2H, phenyl), 6.64−6.62 (dd, J = 3.6, 1.8 Hz, 1H, furoyl), 2.44 (s, 3H, methyl). ^{13}C NMR (100 MHz, $CDCl_3$): δ, ppm 179.1 (C═S), 156.0 (C═O), 146.5 (furoyl), 144.9 (O_2N−C), 142.2 (furoyl), 137.7, 134.1, 129.7, 128.0, 125.3 (phenyl), 119.4, 113.6 (furoyl), 20.9 (methyl).

***N*-((4-methoxy-2-nitrophenyl)carbamothioyl)furan-2-carboxamide (L3).** Yield: 75%. Bright yellow solid. Mp: 168 °C. Anal. Calcd. for $C_{13}H_{11}N_3O_5S$ (%): C, 48.60; H, 3.45; N, 13.08; S, 9.98. Found: C, 48.63; H, 3.47; N, 13.11; S, 10.01. UV−vis (CH_3CN): λ_{max},

https://doi.org/10.1021/acs.inorgchem.3c00757
Inorg. Chem. 2023, 62, 11761−11774

nm (ε, dm^3 mol^{-1} cm^{-1}) 279 (7542), 293 (9939). FT-IR (KBr, cm^{-1}): 3451 (m; ν(amide N−H)), 3135 (s; ν(thioamide N−H)), 1691 (s; ν(C═O)), 1249 (s; ν(C═S)). ^{1}H NMR (400 MHz, $CDCl_3$): δ, ppm 12.89 (s, 1H, O═CNH), 9.32 (s, 1H, S═CNH), 8.20 (d, J = 9.1 Hz, 1H, phenyl), 7.63 (d, J = 1.3 Hz, 1H, furoyl), 7.59 (d, J = 3.0 Hz, 1H, phenyl),7.45 (d, J = 3.6 Hz, 1H, phenyl), 7.22 (dd, J = 9.1, 3.0 Hz, 1H, furoyl), 6.65 (dd, J = 3.6, 1.7 Hz, 1H, furoyl), 3.90 (s, 3H, methoxy). ^{13}C NMR (100 MHz, $CDCl_3$): δ, ppm 179.2 (C═S), 157.9 (C═O), 156.2 (**C**−OCH_3), 146.6 (furoyl), 144.9 (O_2N−C), 143.5 (furoyl), 129.7, 125.2, 120.0 (phenyl), 119.3, 113.6 (furoyl), 109.1 (phenyl), 56.1 (OCH_3).

***N*-((5-chloro-2-nitrophenyl)carbamothioyl)furan-2-carboxamide (L4).** Yield: 79%. Brownish-yellow solid. Mp: 172 °C. Anal. Calcd. for $C_{12}H_8ClN_3O_4S$ (%): C, 44.25; H, 2.48; N, 12.90; S, 9.84. Found: C, 44.21; H, 2.45; N, 12.88; S, 8.82. UV−vis (CH_3CN): λ_{max}, nm (ε, dm^3 mol^{-1} cm^{-1}) 269 (7531), 282 (9930). FT-IR (KBr, cm^{-1}): 3459 (m; ν(amide N−H)), 3119 (s; ν(thioamide N−H)), 1691 (s; ν(C═O)), 1248 (s; ν(C═S)). ^{1}H NMR (400 MHz, $CDCl_3$): δ, ppm 13.33 (s, 1H, O═CNH), 9.34 (s, 1H, S═CNH), 8.67 (d, J = 2.1 Hz, 1H, phenyl), 8.06 (dd, J = 12.2, 9.0 Hz, 2H, phenyl), 7.66−7.39 (m, 2H, furoyl), 6.65−6.63 (dd, J = 4.7, 1.8 Hz, 1H, furoyl). ^{13}C NMR (100 MHz, $CDCl_3$): δ, ppm 179.0 (C═S), 155.9 (C═O), 146.6 (furoyl), 144.7 (O_2N−C), 141.8 (furoyl), 140.0, 133.7, 127.6, 126.3, 119.8 (phenyl), 117.8, 113.6 (furoyl).

***N*-((5-chloro-4-methyl-2-nitrophenyl)carbamothioyl)furan-2-carboxamide (L5).** Yield: 84%. Orange-yellow solid. Mp: 178 °C. Anal. Calcd. for $C_{13}H_{10}ClN_3O_4S$ (%): C, 45.96; H, 2.97; N, 12.37; S, 9.49. Found: C, 45.93; H, 2.92; N, 12.34; S, 9.46. UV−vis (CH_3CN): λ_{max}, nm (ε, dm^3 mol^{-1} cm^{-1}) 261 (7526), 276 (9922). FT-IR (KBr, cm^{-1}): 3451 (m; ν(amide N−H)), 3129 (s; ν(thioamide N−H)), 1679 (s; ν(C═O)), 1251 (s; ν(C═S)). ^{1}H NMR (400 MHz, DMSO-d_6): δ, ppm 12.64 (s, 1H, O═CNH), 11.69 (s, 1H, S═CNH), 8.17 (s, 1H, phenyl), 8.11−7.98 (m, 2H, furoyl), 7.91 (s, 1H, phenyl), 6.78 (dd, J = 3.6, 1.7 Hz, 1H, furoyl), 2.44 (s, 3H, CH_3). ^{13}C NMR (100 MHz, DMSO-d_6): δ, ppm 181.1 (C═S), 158.1 (C═O), 149.2 (furoyl), 144.8 (O_2N−C), 142.7 (furoyl), 138.7, 136.2, 131.5, 130.1, 127.3 (phenyl), 119.9, 113.1 (furoyl), 19.0 (CH_3).

***N*-((4,5-dimethyl-2-nitrophenyl)carbamothioyl)furan-2-carboxamide (L6).** Yield: 88%. Pale yellow solid. Mp: 171 °C. Anal. Calcd. for $C_{14}H_{13}N_3O_4S$ (%): C, 52.66; H, 4.10; N, 13.16; S, 10.04. Found: C, 52.68; H, 4.14; N, 13.19; S, 10.08. UV−vis (CH_3CN): λ_{max}, nm (ε, dm^3 mol^{-1} cm^{-1}) 266 (7529), 281 (9928). FT-IR (KBr, cm^{-1}): 3450 (m; ν(amide N−H)), 3189 (s; ν(thioamide N−H)), 1691 (s; ν(C═O)), 1269 (s; ν(C═S)). ^{1}H NMR (400 MHz, DMSO-d_6): δ, ppm 12.54 (s, 1H, O═CNH), 11.59 (s, 1H, S═CNH), 8.10 (s, 1H, phenyl), 7.99−7.82 (m, 2H, furoyl), 7.68 (s, 1H, phenyl), 6.78 (dd, J = 3.5, 1.6 Hz, 1H, furoyl), 2.50 (s, 3H, CH_3), 2.33 (s, 3H, CH_3). ^{13}C NMR (100 MHz, DMSO-d_6): δ, ppm 180.9 (C═S), 158.1 (C═O), 149.1 (furoyl), 144.9 (O_2N−C), 144.1 (furoyl), 142.1, 137.3, 130.9, 130.1, 125.5 (phenyl), 119.5, 113.1 (furoyl), 19.9 (CH_3), 19.1 (CH_3).

Synthesis of the Ru(II)−Furoylthiourea Complexes. $[RuCl_2(\eta^6\text{-}p\text{-cymene})]_2$ (0.122 g, 0.2 mmol) and the ligand (0.116−0.136 g, 0.4 mmol) (L1−L6) were taken in 10 mL of toluene and stirred for 12 h at 27 °C, forming a clear orange solution. After the completion of reaction as inferred from TLC, the volume of solution was reduced to 2 mL and the addition of petroleum ether (60−80 °C) (10 mL) resulted in an orange solid, which was washed with hexane and dried *in vacuo* to yield complexes **1**−**6**.

$[RuCl_2(\eta^6\text{-}p\text{-cymene})(PPh_3)]$ (0.113 g, 0.1 mmol) and the ligands (0.029−0.033 g, 0.1 mmol) were dissolved in 15 mL of toluene and stirred at room temperature for 20 h. After this, 0.015−0.0025 g of NH_4PF_6 dissolved in methanol was added to the reaction mixture, which was stirred for 4 h. The resultant orange solution was concentrated to 2 mL, and the addition of cold hexane gave a mild orange precipitate, which was filtered, washed with petroleum ether, and dried to yield complexes **7**−**12**.

[Dichloro(*p*-cymene)(*N*-((2-nitrophenyl)carbamothioyl)-furan-2-carboxamide)ruthenium(II)] (1). Yield: 91%. Light orange solid. Mp: 191 °C. Anal. Calcd. for $C_{22}H_{23}Cl_2N_3O_4RuS$ (%): C, 44.23; H, 3.88; N, 7.03; S, 5.37. Found: C, 44.25; H, 3.92; N, 7.06; S, 5.40. UV−vis (CH_2Cl_2): λ_{max}, nm (ε, dm^3 mol^{-1} cm^{-1}) 265 (7539), 285 (7691), 352 (8509), 425 (9648). FT-IR (KBr, cm^{-1}): 3442 (m; ν(amide N−H)), 3139 (s; ν(thioamide N−H)), 1681 (s; ν(C═O)), 1183 (s; ν(C═S)). ^{1}H NMR (400 MHz, $CDCl_3$): δ, ppm 13.15 (s, 1H, O═CNH), 11.25 (s, 1H, S═CNH), 8.12 (d, J = 8.2 Hz, 1H, phenyl), 7.99 (t, J = 5.0 Hz, 2H, phenyl), 7.69 (dd, J = 16.4, 8.1 Hz, 2H, furoyl), 7.51 (t, J = 7.7 Hz, 1H, phenyl), 6.53 (dd, J = 3.6, 1.5 Hz, 1H, furoyl), 5.40 (d, J = 5.9 Hz, 2H, aromatic H of *p*-cymene), 5.24 (d, J = 5.9 Hz, 2H, aromatic H of *p*-cymene), 2.89 (sept, J = 6.9 Hz, 1H, C**H**$(CH_3)_2$), 2.21 (s, 3H, CH_3), 1.28 (d, J = 4.2 Hz, 6H, CH(C**H**$_3)_2$). ^{13}C NMR (100 MHz, $CDCl_3$): δ, ppm 181.0 (C═S), 158.3 (C═O), 148.4 (furoyl), 144.4 (O_2N−C), 143.9 (furoyl), 133.6, 130.8, 128.6, 125.4, 122.4 (phenyl), 112.9 (furoyl), 104.0, 100.0, 84.2, 82.8 (*p*-cymene), 30.5 (**C**H$(CH_3)_2$), 22.1 (CH(**C**H$_3)_2$), 18.3 (CH_3). ESI−MS (m/z) [Found (Calcd.)]: 526.0383 (526.0375) [M − HCl − Cl$^-$]$^+$.

[Dichloro(*p*-cymene)(*N*-((4-methyl-2-nitrophenyl)-carbamothioyl)furan-2-carboxamide)ruthenium(II)] (2). Yield: 82%. Orange solid. Mp: 195 °C. Anal. Calcd. for $C_{23}H_{25}Cl_2N_3O_4RuS$ (%): C, 45.18; H, 4.12; N, 6.87; S, 5.24. Found: C, 45.21; H, 4.14; N, 6.90; S, 5.28. UV−vis (CH_2Cl_2): λ_{max}, nm (ε, dm^3 mol^{-1} cm^{-1}) 269 (7540), 288 (7693), 359 (8514), 431 (9651). FT-IR (KBr, cm^{-1}): 3438 (m; ν(amide N−H)), 3089 (s; ν(thioamide N−H)), 1683 (s; ν(C═O)), 1171 (s; ν(C═S)). ^{1}H NMR (400 MHz, $CDCl_3$): δ, ppm 13.06 (s, 1H, O═CNH), 11.23 (s, 1H, S═CNH), 7.99 (d, J = 3.6 Hz, 1H, phenyl), 7.93 (s, 1H, phenyl), 7.85 (d, J = 8.3 Hz, 1H, furoyl), 7.66 (d, J = 1.5 Hz, 1H, phenyl), 7.49 (d, J = 9.9 Hz, 1H, furoyl), 6.54 (dd, J = 3.7, 1.7 Hz, 1H, furoyl), 5.40 (d, J = 6.0 Hz, 2H, aromatic H of *p*-cymene), 5.24 (d, J = 6.1 Hz, 2H, aromatic H of *p*-cymene), 2.91 (sept, J = 6.9 Hz, 1H, C**H**$(CH_3)_2$), 2.50 (s, 3H, CH_3), 2.22 (s, 3H, CH_3), 1.28 (d, J = 7.0 Hz, 6H, CH(C**H**$_3)_2$). ^{13}C NMR (100 MHz, $CDCl_3$): δ, ppm 181.1 (C═S), 158.6 (C═O), 148.4 (furoyl), 144.7 (O_2N−C), 143.8 (furoyl), 139.4, 134.5, 129.6, 128.4, 125.6 (phenyl), 122.4, 112.9 (furoyl), 104.2, 100.4, 84.9, 82.9 (*p*-cymene), 30.6 (**C**H$(CH_3)_2$), 22.4 (CH(**C**H$_3)_2$), 21.1 (CH_3), 18.3 (CH_3). ESI−MS (m/z) [Found (Calcd.)]: 540.0561 (540.0531) [M − HCl − Cl$^-$]$^+$.

[Dichloro(*p*-cymene)(*N*-((4-methoxy-2-nitrophenyl)-carbamothioyl)furan-2-carboxamide)ruthenium(II)] (3). Yield: 78%. Light orange solid. Mp: 199 °C. Anal. Calcd. for $C_{23}H_{25}Cl_2N_3O_5RuS$ (%): C, 44.02; H, 4.02; N, 6.70; S, 5.11. Found: C, 44.04; H, 4.05; N, 6.73; S, 5.16. UV−vis (CH_2Cl_2): λ_{max}, nm (ε, dm^3 mol^{-1} cm^{-1}) 272 (7542), 294 (7697), 362 (8516), 436 (9655). FT-IR (KBr, cm^{-1}): 3445 (m; ν(amide N−H)), 3123 (s; ν(thioamide N−H)), 1691 (s; ν(C═O)), 1178 (s; ν(C═S)). ^{1}H NMR (400 MHz, $CDCl_3$): δ, ppm 12.92 (s, 1H, O═CNH), 11.23 (s, 1H, S═CNH), 7.99 (d, J = 3.6 Hz, 1H, furoyl), 7.81 (d, J = 9.0 Hz, 1H, phenyl), 7.68−7.58 (m, 2H, phenyl), 7.15 (s, 1H, furoyl), 6.54 (dd, J = 3.6, 1.4 Hz, 1H, furoyl), 5.39 (d, J = 5.9 Hz, 2H, aromatic H of *p*-cymene), 5.23 (d, J = 5.9 Hz, 2H, aromatic H of *p*-cymene), 3.93 (s, 3H, OCH_3), 2.98 (sept, J = 7.4 Hz, 1H, C**H**$(CH_3)_2$), 2.34 (s, 3H, CH_3), 1.31 (d, J = 8.0 Hz, 6H, CH(C**H**$_3)_2$). ^{13}C NMR (100 MHz, $CDCl_3$): δ, ppm 180.8 (C═S), 158.5 (C═O), 148.2 (furoyl), 144.3 (O_2N−C), 131.1 (furoyl), 129.2, 128.1, 125.2 (phenyl), 121.7 (furoyl), 120.1 (phenyl), 112.7 (furoyl), 109.6, 103.7, 100.2, 84.4, 82.7 (*p*-cymene), 56.3 (OCH_3), 30.4, (**C**H$(CH_3)_2$), 22.2 (CH(**C**H$_3)_2$), 18.2 (CH_3). ESI−MS (m/z) [Found (Calcd.)]: 556.0461 (556.0482) [M − HCl − Cl$^-$]$^+$.

[Dichloro(*p*-cymene)(*N*-((5-chloro-2-nitrophenyl)-carbamothioyl)furan-2-carboxamide)ruthenium(II)] (4). Yield: 83%. Bright orange solid. Mp: 205 °C. Anal. Calcd. for $C_{22}H_{22}Cl_3N_3O_4RuS$ (%): C, 41.82; H, 3.51; N, 6.65; S, 5.07. Found: C, 41.78; H, 3.50; N, 6.61; S, 5.05. UV−vis (CH_2Cl_2): λ_{max}, nm (ε, dm^3 mol^{-1} cm^{-1}): 275 (7546), 287 (7694), 365 (8519), 442 (9659). FT-IR (KBr, cm^{-1}): 3430 (m; ν(amide N−H)), 3159 (s; ν(thioamide N−H)), 1691 (s; ν(C═O)), 1178 (s; ν(C═S)). ^{1}H NMR (400 MHz, $CDCl_3$): δ, ppm 13.29 (s, 1H, O═CNH), 11.24 (s, 1H, S═CNH), 8.26−8.02 (m, 2H, phenyl), 7.66 (s, 1H, furoyl), 7.45 (d, J = 8.7 Hz, 1H, furoyl), 7.20 (d, J = 36.0 Hz, 1H, phenyl), 6.53 (dd, J = 4.8, 2.4 Hz, 1H, furoyl), 5.43 (d, J = 3.7 Hz, 2H, aromatic H of *p*-cymene), 5.31 (d, J = 5.6 Hz, 2H, aromatic H of *p*-cymene), 3.04 (sept, J = 6.8 Hz, 1H, C**H**$(CH_3)_2$), 2.23 (s, 3H, CH_3), 1.30 (d, J = 6.8 Hz, 6H, CH(C**H**$_3)_2$). ^{13}C NMR (100 MHz, $CDCl_3$): δ, ppm 181.1 (C═S), 158.5 (C═O),

https://doi.org/10.1021/acs.inorgchem.3c00757
Inorg. Chem. 2023, 62, 11761−11774

148.6 (furoyl) 144.8 (O_2N−C), 140.0 (furoyl), 132.0, 128.9, 128.1, 126.9, 125.5 (phenyl), 122.3, 112.4 (furoyl), 101.4, 97.1, 81.2, 80.6 (*p*-cymene), 30.5 (**C**H(CH_3)$_2$), 22.0 (CH(**C**H_3)$_2$), 19.0 (CH_3). ESI−MS (*m*/*z*) [Found (Calcd.)]: 560.0255 (559.9985) [M − HCl − Cl^-]$^+$.

[Dichloro(*p*-cymene)(*N*-((5-chloro-4-methyl-2-nitrophenyl)-carbamothioyl)furan-2-carboxamide)ruthenium(II)] (5). Yield: 79%. Orange solid. Mp: 194 °C. Anal. Calcd. for $C_{23}H_{24}Cl_3N_3O_4RuS$ (%): C, 42.77; H, 3.75; N, 6.51; S, 4.96. Found: C, 42.74; H, 3.72; N, 6.48; S, 4.92. UV−vis (CH_2Cl_2): λ_{max}, nm (ε, dm^3 mol^{-1} cm^{-1}) 270 (7541), 281 (7690), 358 (8514), 434 (9651). FT-IR (KBr, cm^{-1}): 3442 (m; ν(amide N−H)), 3139 (s; ν(thioamide N−H)), 1681 (s; ν(C═O)), 1179 (s; ν(C═S)). ^{1}H NMR (400 MHz, $CDCl_3$): δ, ppm 13.18 (s, 1H, O═CNH), 12.19 (s, 1H, S═CNH), 8.05 (d, J = 24.6 Hz, 1H, phenyl), 7.99 (s, 1H, phenyl), 7.72 (d, J = 2.8 Hz, 1H, furoyl), 7.65 (d, J = 1.5 Hz, 1H, furoyl), 6.53 (dd, J = 3.7, 1.6 Hz, 1H, furoyl), 5.42 (d, J = 6.1 Hz, 2H, aromatic H of *p*-cymene), 5.26 (d, J = 5.9 Hz, 2H, aromatic H of *p*-cymene), 2.90 (sept, J = 5.7 Hz, 1H, C**H**(CH_3)$_2$), 2.49 (s, 3H, CH_3), 2.23 (s, 3H, CH_3), 1.25 (d, J = 7.0 Hz, 6H, CH(C**H**$_3$)$_2$). ^{13}C NMR (100 MHz, $CDCl_3$): δ, ppm 181.0 (C═S), 158.5 (C═O), 148.7 (furoyl), 144.4 (O_2N−C), 141.6 (furoyl), 140.1, 137.0, 129.7, 127.1 (phenyl), 122.8, 112.9 (furoyl), 104.1 (phenyl), 101.2, 100.5, 84.2, 82.8 (*p*-cymene), 30.7 (**C**H(CH_3)$_2$), 22.0 (CH(**C**H_3)$_2$), 20.1 (CH_3), 18.2 (CH_3). ESI−MS (*m*/*z*) [Found (Calcd.)]: 574.0125 (574.0142) [M − HCl − Cl^-]$^+$.

[Dichloro(*p*-cymene)(*N*-((4,5-dimethyl-2-nitrophenyl)-carbamothioyl)furan-2-carboxamide)ruthenium(II)] (6). Yield: 86%. Dark orange solid. Mp: 201 °C. Anal. Calcd. for $C_{24}H_{27}Cl_2N_3O_4RuS$ (%): C, 46.08; H, 4.35; N, 6.72; S, 5.13. Found: C, 46.12; H, 4.36; N, 6.74; S, 5.17. UV−vis (CH_2Cl_2): λ_{max}, nm (ε, dm^3 mol^{-1} cm^{-1}) 275 (7546), 286 (7694), 362 (8517), 439 (9658). FT-IR (KBr, cm^{-1}): 3438 (m; ν(amide N−H)), 3115 (s; ν(thioamide N−H)), 1691 (s; ν(C═O)), 1187 (s; ν(C═S)). ^{1}H NMR (400 MHz, $CDCl_3$): δ, ppm 12.94 (s, 1H, O═CNH), 11.19 (s, 1H, S═CNH), 7.93 (d, J = 3.6 Hz, 1H, furoyl), 7.87 (s, 1H, phenyl), 7.64 (s, 1H, furoyl), 7.60 (s, 1H, phenyl), 6.49 (dd, J = 3.6, 1.6 Hz, 1H, furoyl), 5.35 (d, J = 5.9 Hz, 2H, aromatic H of *p*-cymene), 5.19 (d, J = 5.9 Hz, 2H, aromatic H of *p*-cymene), 2.93 (sept, J = 5.2 Hz, 1H, C**H**(CH_3)$_2$), 2.32 (d, J = 5.3 Hz, 6H, CH_3), 2.16 (s, 3H, CH_3), 1.23 (d, J = 6.9 Hz, 6H, CH(C**H**$_3$)$_2$). ^{13}C NMR (100 MHz, $CDCl_3$): δ, ppm 180.7 (C═S), 158.1 (C═O), 148.1 (furoyl), 144.5 (O_2N−C), 143.9 (furoyl), 141.4, 137.8, 130.5, 128.3, 126.0 (phenyl), 121.8, 113.0 (furoyl), 103.7, 100.0, 84.1, 82.8 (*p*-cymene), 30.4 (**C**H(CH_3)$_2$), 22.2 (CH(**C**H_3)$_2$), 19.9 (CH_3), 19.4 (CH_3), 18.2 (CH_3). ESI−MS (*m*/*z*) [Found (Calcd.)]: 554.0729 (554.0688) [M − HCl − Cl^-]$^+$.

[Chlorotriphenylphosphine(*p*-cymene)(*N*-((2-nitrophenyl)-carbamothioyl)furan-2-carboxamide)ruthenium(II)]-hexaflurophosphate (7). Yield: 81%. Pale orange solid. Mp: 210 °C. Anal. Calcd. for $C_{40}H_{38}ClN_3O_4PRuS$ (%): C, 58.28; H, 4.65; N, 5.10; S, 3.89. Found: C, 58.32; H, 4.67; N, 5.13; S, 3.92. UV−vis (CH_3CN): λ_{max}, nm (ε, dm^3 mol^{-1} cm^{-1}) 263 (7536), 275 (7685), 350 (8510), 449 (9642). FT-IR (KBr, cm^{-1}): 3430 (m; ν(amide N−H)), 3166 (s; ν(thioamide N−H)), 1695 (s; ν(C═O)), 1186 (s; ν(C═S)), 1437, 1092 and 710 (s; ν(PPh_3)). ^{1}H NMR (400 MHz, $CDCl_3$): δ, ppm 12.97 (s, 1H, O═CNH), 11.83 (s, 1H, S═CNH), 7.89 (d, J = 1.2 Hz, 1H, furoyl), 7.75 (dd, J = 1.7, 0.7 Hz, 1H, phenyl), 7.60 (dd, J = 3.7, 0.7 Hz, 1H, furoyl), 7.52−7.38 (m, 15H, H of PPh_3), 7.36 (dd, J = 2.8, 1.2 Hz, 3H, phenyl), 6.68 (dd, J = 3.7, 1.7 Hz, 1H, furoyl), 5.62 (d, J = 6.4 Hz, 2H, aromatic H of *p*-cymene), 5.40 (dd, J = 78.0, 6.3 Hz, 2H, aromatic H of *p*-cymene), 2.67 (sept, J = 4.4 Hz, 1H, C**H**(CH_3)$_2$), 2.49 (s, 3H, CH(C**H**$_3$)$_2$), 1.89 (s, 3H, CH(C**H**$_3$)$_2$), 1.62 (s, 3H, CH_3). ^{13}C NMR (100 MHz, $CDCl_3$): δ, ppm 181.4 (C═S), 158.3 (C═O), 147.8 (O_2N−C), 144.4 (furoyl), 143.6 (phenyl), 140.7 (furoyl), 135.5 (phenyl), 131.6, 130.2, 129.7 (C of PPh_3), 128.6 (phenyl), 127.0 (C of PPh_3), 125.8 (furoyl), 121.2, 115.7 (phenyl), 113.8 (furoyl), 93.6, 92.1, 91.0, 89.7 (*p*-cymene), 30.8 (**C**H(CH_3)$_2$), 21.2 (CH(**C**H_3)$_2$), 17.4 (CH_3). ^{31}P NMR (162 MHz, $CDCl_3$): δ, ppm 30.82 (PPh_3), −130.7, −135.2, −139.3, −143.7, −148.0, −152.7, −156.2 (PF_6). ESI−MS (*m*/*z*) [Found (Calcd.)]: 824.3133 (824.3148) [M − PF_6^-]$^+$.

[Chlorotriphenylphosphine(*p*-cymene)(*N*-((4-methyl-2-nitrophenyl)carbamothioyl)furan-2-carboxamide)ruthenium-(II)]hexaflurophosphate (8). Yield: 77%. Orange solid. Mp: 215 °C. Anal. Calcd. for $C_{41}H_{40}ClN_3O_4PRuS$ (%): C, 58.74; H, 4.81; N, 5.01; S, 3.82. Found: C, 58.71; H, 4.76; N, 4.98; S, 3.78. UV−vis (CH_3CN): λ_{max}, nm (ε, dm^3 mol^{-1} cm^{-1}) 268 (7539), 281 (7690), 359 (8514), 459 (9648). FT-IR (KBr, cm^{-1}): 3430 (m; ν(amide N−H)), 3159 (s; ν(thioamide N−H)), 1700 (s; ν(C═O)), 1183 (s; ν(C═S)), 1445, 1076 and 721 (s; ν(PPh_3)). ^{1}H NMR (400 MHz, $CDCl_3$): δ, ppm 13.17 (s, 1H, O═CNH), 9.32 (s, 1H, S═CNH), 8.46 (d, J = 8.3 Hz, 1H, phenyl), 8.10 (d, J = 8.3 Hz, 1H, furoyl), 7.83 (s, 1H, phenyl), 7.78 (s, 1H, phenyl), 7.62 (d, J = 2.5 Hz, 1H, furoyl), 7.40−7.29 (m, 15H, H of PPh_3), 6.71 (dd, J = 3.9, 1.4 Hz, 1H, furoyl), 5.19 (dd, J = 9.9, 6.3 Hz, 2H, aromatic H of *p*-cymene), 4.98 (dd, J = 10.2, 8.4 Hz, 2H, aromatic H of *p*-cymene), 2.82 (sept, J = 5.9 Hz, 1H, C**H**(CH_3)$_2$), 1.85 (s, 3H, CH_3), 1.08 (d, J = 7.0 Hz, 9H, CH(C**H**$_3$)$_2$; CH_3). ^{13}C NMR (100 MHz, $CDCl_3$): δ, ppm 179.3 (C═S), 156.1 (C═O), 146.5 (O_2N═C), 144.9, 134.5 (furoyl), 134.3 (phenyl), 134.1 (furoyl), 133.6 (phenyl), 130.3, 130.2, 128.1 (C of PPh_3), 127.9 (phenyl), 127.0 (C of PPh_3), 125.2 (furoyl), 119.6, 113.6 (phenyl), 111.0 (furoyl), 96.2, 88.9, 87.1, 79.7 (*p*-cymene), 22.5 (**C**H(CH_3)$_2$), 22.3 (CH(**C**H_3)$_2$), 17.6 (CH_3). ^{31}P NMR (162 MHz, $CDCl_3$): δ, ppm 26.81 (PPh_3), −131.5, −134.3, −138.3, −143.8, −149.1, −151.8, −157.6 (PF_6). ESI−MS (*m*/*z*) [Found (Calcd.)]: 838.1241 (838.1249) [M − PF_6^-]$^+$.

[Chlorotriphenylphosphine(*p*-cymene)(*N*-((4-methoxy-2-nitrophenyl)carbamothioyl)furan-2-carboxamide)ruthenium-(II)]hexafluorophosphate (9). Yield: 81%. Orange solid. Mp: 221 °C. Anal. Calcd. for $C_{41}H_{40}ClN_3O_5PRuS$ (%): C, 57.64; H, 4.72; N, 4.92; S, 3.75. Found: C, 57.60; H, 4.70; N, 4.88; S, 3.72. UV−vis (CH_3CN): λ_{max}, nm (ε, dm^3 mol^{-1} cm^{-1}) 260 (7530), 275 (7686), 354 (8510), 452 (9644). FT-IR (KBr, cm^{-1}): 3426 (m; ν(amide N−H)), 3140 (s; ν(thioamide N−H)), 1685 (s; ν(C═O)), 1184 (s; ν(C═S)), 1451, 1092 and 715 (s; ν(PPh_3)). ^{1}H NMR (400 MHz, $CDCl_3$): δ, ppm 12.83 (s, 1H, O═CNH), 11.84 (s, 1H, S═CNH), 7.85 (s, 1H, phenyl), 7.82 (d, J = 4.6 Hz, 1H, furoyl), 7.80 (s, 1H, phenyl), 7.76 (s, 1H, phenyl), 7.62 (s, 1H, furoyl), 7.45−7.33 (m, 15H, H of PPh_3), 6.69 (dd, J = 3.6, 1.6 Hz, 1H, furoyl), 5.20 (d, J = 6.1 Hz, 2H, aromatic H of *p*-cymene), 5.00 (d, J = 5.5 Hz, 2H, aromatic H of *p*-cymene), 3.95 (s, 3H, OCH_3), 2.93 (sept, 1H, J = 5.8 Hz, C**H**(CH_3)$_2$), 1.89 (d, J = 10.4 Hz, 6H, CH(C**H**$_3$)$_2$), 1.18 (s, 3H, CH_3). ^{13}C NMR (100 MHz, $CDCl_3$): δ, ppm 181.3 (C═O), 159.9 (C═S), 147.9 (O_2N−C), 144.8 (furoyl), 144.4 (phenyl), 134.3 (furoyl), 133.7 (phenyl), 131.6, 131.0 (C of PPh_3), 130.3 (phenyl), 128.6, 128.0 (C of PPh_3), 122.2 (phenyl), 113.7, 111.2 (furoyl), 110.6 (phenyl), 102.3, 95.7, 88.9, 87.1 (*p*-cymene), 56.7 (OCH_3), 30.7 (**C**H(CH_3)$_2$), 21.6 (CH(**C**H_3)$_2$), 17.2 (CH_3). ^{31}P NMR (162 MHz, $CDCl_3$): δ, ppm 30.78 (PPh_3), −130.9, −135.4, −139.9, −144.4, −148.3, −152.3, −157.0 (PF_6). ESI−MS (*m*/*z*) [Found (Calcd.)]: 854.1289 (854.1297) [M − PF_6^-]$^+$.

[Chlorotriphenylphosphine(*p*-cymene)(*N*-((5-chloro-2-nitrophenyl)carbamothioyl)furan-2-carboxamide)ruthenium-(II)]hexaflurophosphate (10). Yield: 76%. Bright orange solid. Mp: 216 °C. Anal. Calcd. for $C_{40}H_{37}Cl_2N_3O_4PRuS$ (%): C, 55.95; H, 4.34; N, 4.89; S, 3.73. Found: C, 55.99; H, 4.37; N, 4.93; S, 3.76. UV−vis (CH_3CN): λ_{max}, nm (ε, dm^3 mol^{-1} cm^{-1}) 250 (7523), 262 (7679), 343 (8501), 444 (9638). FT-IR (KBr, cm^{-1}): 3446 (m; ν(amide N−H)), 3125 (s; ν(thioamide N−H)), 1683 (s; ν(C═O)), 1187 (s; ν(C═S)), 1452, 1081 and 715 (s; ν(PPh_3)). ^{1}H NMR (400 MHz, $CDCl_3$): δ, ppm 12.97 (s, 1H, O═CNH), 11.85 (s, 1H, S═CNH), 7.90 (s, 1H, phenyl), 7.85−7.78 (m, 1H, furoyl), 7.77 (s, 1H, phenyl), 7.60 (d, J = 2.9 Hz, 1H, phenyl), 7.49 (s, 1H, furoyl), 7.49−7.19 (m, 15H, H of PPh_3), 6.67 (dd, J = 16.0, 2.9 Hz, 1H, furoyl), 5.57 (d, J = 7.6 Hz, 2H, aromatic H of *p*-cymene), 5.10 (d, J = 5.9 Hz, 2H, aromatic H of *p*-cymene), 2.99 (sept, J = 5.4 Hz, 1H, C**H**(CH_3)$_2$), 2.50 (s, 3H, CH_3), 1.14 (d, J = 7.6 Hz, 6H, CH(C**H**$_3$)$_2$). ^{13}C NMR (100 MHz, $CDCl_3$): δ, ppm 178.9 (C═S), 155.9 (C═O), 146.7 (O_2N−C), 144.6 (furoyl), 140.0 (phenyl), 134.4 (furoyl), 134.3, 133.6 (phenyl), 130.3, 130.2 (C of PPh_3), 128.0 (phenyl), 127.9 (C of PPh_3), 119.8 (phenyl), 113.6, 111.4 (furoyl), 95.9 (phenyl), 89.1, 89.0, 87.2, 87.0 (*p*-cymene), 30.3 (**C**H(CH_3)$_2$), 22.0 (CH(**C**H_3)$_2$), 17.8 (CH_3). ^{31}P NMR (162 MHz, $CDCl_3$): δ, ppm 28.48 (PPh_3), −132.5, −136.4, −139.3, −143.8, −147.8, −152.3, −155.7 (PF_6). ESI−MS (*m*/*z*) [Found (Calcd.)]: 858.7560 (858.7568) [M − PF_6^-]$^+$.

https://doi.org/10.1021/acs.inorgchem.3c00757
Inorg. Chem. 2023, 62, 11761−11774

[Chlorotriphenylphosphine(*p*-cymene)(*N*-((5-chloro-4-methyl-2-nitrophenyl)carbamothioyl)furan-2-carboxamide)-ruthenium(II)]hexaflurophosphate (11). Yield: 80%. Bright orange solid. Mp: 224 °C. Anal. Calcd. for $C_{41}H_{39}Cl_2N_3O_4PRuS$ (%): C, 56.42; H, 4.50; N, 4.81; S, 3.67. Found: C, 56.38; H, 4.48; N, 4.77; S, 3.63. UV−vis (CH_3CN): λ_{max}, nm (ε, $dm^3\ mol^{-1}\ cm^{-1}$) 258 (7529), 265 (7680), 347 (8506), 449 (9640). FT-IR (KBr, cm^{-1}): 3434 (m; ν(amide N−H)), 3131 (s; ν(thioamide N−H)), 1689 (s; ν(C═O)), 1171 (s; ν(C═S)), 1441, 1087 and 720 (s; $\nu(PPh_3)$). ^{1}H NMR (400 MHz, $CDCl_3$): δ, ppm 13.11 (s, 1H, O═CNH), 11.96 (s, 1H, S═CNH), 8.02 (s, 1H, phenyl), 7.81 (dd, J = 12.8, 7.7 Hz, 1H, furoyl), 7.70−7.59 (m, 1H, phenyl), 7.60−7.35 (m, 15H, H of PPh_3), 6.74 (dd, J = 10.0, 2.4 Hz, 1H, furoyl), 5.74 (d, J = 13.8 Hz, 2H, aromatic H of *p*-cymene), 5.45 (d, J = 21.9 Hz, 2H, aromatic H of *p*-cymene), 2.96 (sept, J = 5.9 Hz, 1H, C**H**$(CH_3)_2$), 2.50 (s, 3H, CH_3), 1.97 (s, 3H, CH_3), 1.14 (d, J = 6.7 Hz, 6H, CH(C**H**$_3)_2$). ^{13}C NMR (100 MHz, $CDCl_3$): δ, ppm 179.5 (C═S), 157.8 (C═O), 146.5 (O_2N−C), 145.0 (furoyl), 134.4 (phenyl), 134.2 (furoyl), 131.2 (phenyl), 130.2, 129.9 (C of PPh_3), 128.5 (phenyl), 128.5 (C of PPh_3), 127.9 (phenyl), 127.9, 125.3 (furoyl), 119.9 (phenyl), 119.4 (furoyl), 109.3, 95.8, 89.1, 87.3 (*p*-cymene), 30.7 (**C**H$(CH_3)_2$), 30.4 (CH(**C**H$_3)_2$), 21.5 (CH_3), 17.4 (CH_3). ^{31}P NMR (162 MHz, $CDCl_3$): δ, ppm 29.83 (PPh_3), −133.5, −137.1, −140.7, −144.3, −147.7, −151.2, −154.7 (PF_6). ESI−MS (m/z) [Found (Calcd.)]: 872.0833 (872.0840) [M − PF_6^-]$^+$.

[Chlorotriphenylphosphine(*p*-cymene)(*N*-((4,5-dimethyl-2-nitrophenyl)carbamothioyl)furan-2-carboxamide)ruthenium-(II)]hexaflurophosphate (12). Yield: 83%. Light orange solid. Mp: 219 °C. Anal. Calcd. for $C_{42}H_{42}ClN_3O_4PRuS$ (%): C, 59.18; H, 4.97; N, 4.93; S, 3.76. Found: C, 59.20; H, 5.00; N, 4.97; S, 3.79. UV−vis (CH_3CN): λ_{max}, nm (ε, $dm^3\ mol^{-1}\ cm^{-1}$) 261 (7531), 272 (7685), 351 (8509), 454 (9645). FT-IR (KBr, cm^{-1}): 3454 (m; ν(amide N−H)), 3131 (s; ν(thioamide N−H)), 1691 (s; ν(C═O)), 1171 (s; ν(C═S)), 1441, 1089 and 720 (s; $\nu(PPh_3)$). ^{1}H NMR (400 MHz, $CDCl_3$): δ, ppm 13.00 (s, 1H, O═CNH), 11.91 (s, 1H, S═CNH), 7.92 (s, 1H, phenyl), 7.84 (d, J = 10.1 Hz, 1H, furoyl), 7.77 (s, 1H, phenyl), 7.63 (d, J = 3.6 Hz, 1H, furoyl), 7.50−7.33 (m, 15H, H of PPh_3), 6.70 (dd, J = 3.7, 1.7 Hz, 1H, furoyl), 5.66 (d, J = 10.7 Hz, 2H, aromatic H of *p*-cymene), 5.41 (d, J = 6.2 Hz, 2H, aromatic H of *p*-cymene), 2.61 (sept, J = 6.4 Hz, 1H, C**H**$(CH_3)_2$), 2.40 (s, 3H, CH_3), 2.30 (s, 3H, CH_3), 1.93 (s, 3H, CH_3), 1.12 (d, J = 6.9 Hz, 6H, CH(C**H**$_3)_2$). ^{13}C NMR (100 MHz, $CDCl_3$): δ, ppm 181.4 (C═S), 158.2 (C═O), 147.8 (O_2N−C), 145.2 (furoyl), 144.1 (phenyl), 141.7 (furoyl), 139.3 (phenyl), 131.8, 131.2 (C of PPh_3), 130.6 (phenyl), 128.6 (C of PPh_3), 128.5 (phenyl), 128.4, 126.4 (furoyl), 113.7 (phenyl), 102.3 (furoyl), 93.5, 92.3, 89.2, 87.2 (*p*-cymene), 30.9 (**C**H$(CH_3)_2$), 22.2 (CH(**C**H$_3)_2$), 21.5 (CH_3), 19.9 (CH_3), 19.7 (CH_3). ^{31}P NMR (162 MHz, $CDCl_3$): δ, ppm 30.3 (PPh_3), −130.5, −135.6, −139.3, −144.5, −147.3, −152.6, −156.6 (PF_6). ESI−MS (m/z) [Found (Calcd.)]: 852.3681 (852.3688) [M − PF_6^-]$^+$.

■ ASSOCIATED CONTENT

Supporting Information

The Supporting Information is available free of charge at https://pubs.acs.org/doi/10.1021/acs.inorgchem.3c00757.

Procedures for biomolecular interactions and biological studies; spectra and microscopic images; crystal data and structure refinement details for ligands L2 and L3, and complexes **1**, **3**, **4** and **6**; and rate constants and half-life periods for complexes **1**−**12** (PDF)

2217793−2217798 (1) (ZIP)

Accession Codes

CCDC 2217793−2217798 contain the supplementary crystallographic data for this paper. These data can be obtained free of charge via www.ccdc.cam.ac.uk/data_request/cif, or by emailing data_request@ccdc.cam.ac.uk, or by contacting The Cambridge Crystallographic Data Centre, 12 Union Road, Cambridge CB2 1EZ, UK; fax: +44 1223 336033.

■ AUTHOR INFORMATION

Corresponding Author

Ramasamy Karvembu − *Department of Chemistry, National Institute of Technology, Tiruchirappalli 620015, India;* orcid.org/0000-0001-8966-8602; Email: kar@nitt.edu

Authors

Dorothy Priyanka Dorairaj − *Department of Chemistry, National Institute of Technology, Tiruchirappalli 620015, India*

Jebiti Haribabu − *Faculty of Medicine, University of Atacama, 1532502 Copiapo, Chile;* orcid.org/0000-0001-8855-032X

Mahendiran Dharmasivam − *Department of Chemistry, Griffith Institute for Drug Discovery, Griffith University, Brisbane, Queensland 4111, Australia*

Rahime Eshaghi Malekshah − *Medical Biomaterial Research Centre (MBRC), Tehran University of Medical Sciences, Tehran 1416634793, Iran*

Mohamed Kasim Mohamed Subarkhan − *The First Affiliated Hospital, Key Laboratory of Combined Multi-Organ Transplantation, Ministry of Public Health, School of Medicine, Zhejiang University, Hangzhou 310018, P. R. China;* orcid.org/0000-0002-1164-478X

Cesar Echeverria − *Faculty of Medicine, University of Atacama, 1532502 Copiapo, Chile*

Complete contact information is available at: https://pubs.acs.org/10.1021/acs.inorgchem.3c00757

Notes

The authors declare no competing financial interest.

■ ACKNOWLEDGMENTS

D.P.D. thanks the Department of Science and Technology, Ministry of Science and Technology, Government of India, for the DST-INSPIRE doctoral fellowship (IF170457). J.H. thanks the Fondo Nacional de Ciencia y Tecnologia (FONDECYT, Project Nos. 3200391 and 11170840) for the post-doctoral fellowship. R.K. thanks the DST-SERB for financial assistance (CRG/2022/003145).

■ REFERENCES

(1) Fahad Ullah, M. Breast cancer: Current perspectives on the disease status. In *Breast Cancer Metastasis and Drug Resistance: Challenges and Progress*; Springer International Publishing, 2019; pp 51−64.

(2) Florea, A. M.; Büsselberg, D. Cisplatin as an anti-tumor drug: Cellular mechanisms of activity, drug resistance and induced side effects. *Cancers* **2011**, *3*, 1351−1371.

(3) Segal, E.; Le Pecq, J.-B. Role of ligand exchange processes in the reaction kinetics of the antitumor drug *cis*-diamminedichloroplatinum-(II) with its targets. *Cancer Res.* **1985**, *45*, 492−498.

(4) Motswainyana, W. M.; Ajibade, P. A. Anticancer activities of mononuclear ruthenium(II) coordination complexes. *Adv. Chem.* **2015**, *2015*, 1−21.

(5) Clarke, M. Oncological implications of the chemistry of ruthenium. *Met. Ions Biol. Syst.* **1980**, *11*, 231−283.

(6) Novakova, O.; Kasparkova, J.; Vrana, O.; Van Vliet, P. M.; Reedijk, J.; Brabec, V. Correlation between cytotoxicity and DNA binding of polypyridyl ruthenium complexes. *Biochemistry* **1995**, *34*, 12369−12378.

(7) Keppler, B. K.; Rupp, W.; Juhl, U.; Endres, H.; Niebl, R.; Balzer, W. Synthesis, molecular structure and tumor-inhibiting properties of imidazolium *trans-bis*(imidazole)tetrachlororuthenate(III) and its methyl-substituted derivatives. *Inorg. Chem.* **1987**, *26*, 4366−4370.

(8) Alessio, E. Thirty years of the drug candidate NAMI-A and the myths in the field of ruthenium anticancer compounds: A personal perspective. *Eur. J. Inorg. Chem.* **2017**, *2017*, 1549−1560.
(9) Alessio, E.; Messori, L. NAMI-A and KP1019/1339, two iconic ruthenium anticancer drug candidates face-to-face: A case story in medicinal inorganic chemistry. *Molecules* **2019**, *24*, 1995−2016.
(10) Alessio, E.; Mestroni, G.; Bergamo, A.; Sava, G. Ruthenium antimetastatic agents. *Curr. Top. Med. Chem.* **2004**, *4*, 1525−1535.
(11) Vock, C. A.; Scolaro, C.; Phillips, A. D.; Scopelliti, R.; Sava, G.; Dyson, P. J. Synthesis, characterization and *in vitro* evaluation of novel ruthenium(II) η^6-arene imidazole complexes. *J. Med. Chem.* **2006**, *49*, 5552−5561.
(12) Sava, G.; Pacor, S.; Bregant, F.; Ceschia, V.; Mestroni, G. Metal complexes of ruthenium: Antineoplastic properties and perspectives. *Anti-Cancer Drugs* **1990**, *1*, 99−108.
(13) Rademaker-Lakhai, J. M.; Van den Bongard, D.; Pluim, D.; Beijnen, J. H.; Schellens, J. H. M. A phase I and pharmacological study with imidazolium-*trans*-DMSO-imidazole-tetrachlororuthenate; A novel ruthenium anticancer agent. *Clin. Cancer Res.* **2004**, *10*, 3717−3727.
(14) Monro, S.; Colón, K. L.; Yin, H.; Roque, J., III; Konda, P.; Gujar, S.; Thummel, R. P.; Lilge, L.; Cameron, C. G.; McFarland, S. A. Transition metal complexes and photodynamic therapy from a tumor-centered approach: Challenges, opportunities and highlights from the development of TLD1433. *Chem. Rev.* **2019**, *119*, 797−828.
(15) Karges, J. Clinical development of metal complexes as photosensitizers for photodynamic therapy of cancer. *Angew. Chem., Int. Ed.* **2022**, *61*, No. e202112236.
(16) Dale, L.; Tocher, J.; Dyson, T.; Edwards, D.; Tocher, D. Studies on DNA damage and induction of SOS repair by novel multifunctional bioreducible compounds. II. A metronidazole adduct of a ruthenium-arene compound. *Anti-Cancer Drug Des.* **1992**, *7*, 3−14.
(17) Habtemariam, A.; Melchart, M.; Fernández, R.; Parsons, S.; Oswald, I. D.; Parkin, A.; Fabbiani, F. P.; Davidson, J. E.; Dawson, A.; Aird, R. E.; et al. Structure-activity relationships for cytotoxic ruthenium(II) arene complexes containing *N,N*-, *N,O*-, and *O,O*-chelating ligands. *J. Med. Chem.* **2006**, *49*, 6858−6868.
(18) Morris, R. E.; Aird, R. E.; del Socorro Murdoch, P.; Chen, H.; Cummings, J.; Hughes, N. D.; Parsons, S.; Parkin, A.; Boyd, G.; Jodrell, D. I.; Sadler, P. J. Inhibition of cancer cell growth by ruthenium(II) arene complexes. *J. Med. Chem.* **2001**, *44*, 3616−3621.
(19) Yan, Y. K.; Melchart, M.; Habtemariam, A.; Sadler, P. J. Organometallic chemistry, biology and medicine: Ruthenium arene anticancer complexes. *Chem. Commun.* **2005**, *38*, 4764−4776.
(20) Correa, R. S.; de Oliveira, K. M.; Delolo, F. G.; Alvarez, A.; Mocelo, R.; Plutin, A. M.; Cominetti, M. R.; Castellano, E. E.; Batista, A. A. Ru(II)-based complexes with *N*-(acyl)-*N*′, *N*′-(disubstituted) thiourea ligands: Synthesis, characterization, BSA-and DNA-binding studies of new cytotoxic agents against lung and prostate tumour cells. *J. Inorg. Biochem.* **2015**, *150*, 63−71.
(21) Cunha, B. N.; Colina-Vegas, L.; Plutin, A. M.; Silveira, R. G.; Honorato, J.; Oliveira, K. M.; Cominetti, M. R.; Ferreira, A. G.; Castellano, E. E.; Batista, A. A. Hydrolysis reaction promotes changes in coordination mode of Ru(II)/acylthiourea organometallic complexes with cytotoxicity against human lung tumor cell lines. *J. Inorg. Biochem.* **2018**, *186*, 147−156.
(22) Cunha, B. N.; Luna-Dulcey, L.; Plutin, A. M.; Silveira, R. G.; Honorato, J.; Cairo, R. R.; de Oliveira, T. D.; Cominetti, M. R.; Castellano, E. E.; Batista, A. A. Selective coordination mode of acylthiourea ligands in half-sandwich Ru(II) complexes and their cytotoxic evaluation. *Inorg. Chem.* **2020**, *59*, 5072−5085.
(23) de Oliveira, T. D.; Plutín, A. M.; Luna-Dulcey, L.; Castellano, E. E.; Cominetti, M. R.; Batista, A. A. Cytotoxicity of ruthenium-*N,N*-disubstituted-*N*′-acylthioureas complexes. *Mater. Sci. Eng. C* **2020**, *115*, No. 111106.
(24) Dorairaj, D. P.; Haribabu, J.; Chithravel, V.; Vennila, K. N.; Bhuvanesh, N.; Echeverria, C.; Hsu, S. C. N.; Karvembu, R. Spectroscopic, anticancer and antioxidant studies of fluxional *trans*-$[PdCl_2(S\text{-acylthiourea})_2]$ complexes. *Results Chem.* **2021**, *3*, No. 100157.
(25) Nkabyo, H. A.; Barnard, I.; Koch, K. R.; Luckay, R. C. Recent advances in the coordination and supramolecular chemistry of monopodal and bipodal acylthiourea-based ligands. *Coord. Chem. Rev.* **2021**, *427*, No. 213588.
(26) Dago, A.; Simonov, M.; Pobedimskaya, E.; Martin, A.; Masia, A. Crystal structure of furoyl-1(*o*-nitro)-3-phenylthiourea ($C_{12}H_9N_3O_4S$). *Kristallografiya* **1987**, *32*, 1024−1026.
(27) Dorairaj, D. P.; Haribabu, J.; Shashankh, P. V. S.; Chang, Y.-L.; Echeverria, C.; Hsu, S. C. N.; Karvembu, R. Bidentate acylthiourea ligand anchored Pd-PPh_3 complexes with biomolecular binding, cytotoxic, antioxidant and antihemolytic properties. *J. Inorg. Biochem.* **2022**, *233*, No. 111843.
(28) Dorairaj, D. P.; Haribabu, J.; Chang, Y. L.; Echeverria, C.; Hsu, S. C. N.; Karvembu, R. Pd(II)−PPh_3 complexes of halogen substituted acylthiourea ligands: Biomolecular interactions and *in vitro* anti-proliferative activity. *Appl. Organomet. Chem.* **2022**, *36*, No. e6765.
(29) Biancalana, L.; Zacchini, S.; Ferri, N.; Lupo, M. G.; Pampaloni, G.; Marchetti, F. Tuning the cytotoxicity of ruthenium(II) *para*-cymene complexes by mono-substitution at a triphenylphosphine/phenoxydiphenylphosphine ligand. *Dalton Trans.* **2017**, *46*, 16589−16604.
(30) Rajasekaran, H.; Jerome, P.; Eliseenkov, E. V.; Boyarskiy, V. P.; Bhuvanesh, N. S. P.; Karvembu, R. Half-sandwich Ru(II)-thioamide complexes as catalysts for one pot synthesis of aromatic 1, 5-diketones. *J. Organomet. Chem.* **2022**, *965-966*, No. 122322.
(31) Obradović, D.; Nikolić, S.; Milenković, I.; Milenković, M.; Jovanović, P.; Savić, V.; Roller, A.; Crnogorac, MĐ.; Stanojković, T.; Grgurić-Šipka, S. Synthesis, characterization, antimicrobial and cytotoxic activity of novel half-sandwich Ru(II) arene complexes with benzoylthiourea derivatives. *J. Inorg. Biochem.* **2020**, *210*, No. 111164.
(32) Parveen, S.; Tong, K. K.; Rauf, M. R.; Kubanik, M.; Shaheen, M. A.; Söhnel, T.; Jamieson, S. M.; Hanif, M.; Hartinger, C. G. Coordination chemistry of organoruthenium compounds with benzoylthiourea ligands and their biological properties. *Chem. Asian J.* **2019**, *14*, 1262−1270.
(33) Swaminathan, S.; Haribabu, J.; Subarkhan, M. K. M.; Manonmani, G.; Senthilkumar, K.; Balakrishnan, N.; Bhuvanesh, N. S. P.; Echeverria, C.; Karvembu, R. Coordination behavior of acylthiourea ligands in their Ru(II)−benzene complexes-Structures and anticancer activity. *Organometallics* **2022**, *41*, 1621−1630.
(34) Rohini, G.; Konakanchi, R.; Jyothi, P.; Bhuvanesh, N. S. P.; Anandaram, S. Unusual coordination mode of aroyl/acyl thiourea ligands and their π-arene ruthenium(II) piano-stool complexes: Synthesis, molecular geometry, theoretical studies and biological applications. *Appl. Organomet. Chem.* **2019**, *33*, No. e4899.
(35) Yadav, S.; Vijayan, P.; Gupta, R. Ruthenium complexes of *N*/*O*/*S* based multidentate ligands: Structural diversities and catalysis perspectives. *J. Organomet. Chem.* **2021**, *954-955*, No. 122081.
(36) Hansda, S.; Mitra, A.; Ghosh, R. Studies to explore the UVA photosensitizing action of 9-phenylacridine in cells by interaction with DNA. *Nucleosides, Nucleotides Nucleic Acids* **2021**, *40*, 393−422.
(37) Ramachandran, E.; Kalaivani, P.; Prabhakaran, R.; Rath, N. P.; Brinda, S.; Poornima, P.; Padma, V. V.; Natarajan, K. Synthesis, X-ray crystal structure, DNA binding, antioxidant and cytotoxicity studies of Ni(II) and Pd(II) thiosemicarbazone complexes. *Metallomics* **2012**, *4*, 218−227.
(38) Zhou, Q.-X.; Yang, F.; Lei, W.-H.; Chen, J.-R.; Li, C.; Hou, Y.-J.; Ai, X.-C.; Zhang, J.-P.; Wang, X.-S.; Zhang, B.-W. Ruthenium(II) terpyridyl complexes exhibiting DNA photocleavage: The role of the substituent on monodentate ligand. *J. Phys. Chem. B.* **2009**, *113*, 11521−11526.
(39) Lee, M.; Rhodes, A. L.; Wyatt, M. D.; Forrow, S.; Hartley, J. A. GC base sequence recognition by oligoimidazolecarboxamide and C-terminus-modified analogs of distamycin deduced from circular dichroism, proton nuclear magnetic resonance, and methidiumpropyl-lethylenediaminetetraacetate-iron(II) footprinting studies. *Biochemistry* **1993**, *32*, 4237−4245.

https://doi.org/10.1021/acs.inorgchem.3c00757
Inorg. Chem. 2023, 62, 11761−11774

(40) Suh, D.; Chaires, J. B. Criteria for the mode of binding of DNA binding agents. *Bioorg. Med. Chem.* **1995**, *3*, 723−728.
(41) Kellett, A.; Molphy, Z.; Slator, C.; McKee, V.; Farrell, N. P. Molecular methods for assessment of non-covalent metallodrug-DNA interactions. *Chem. Soc. Rev.* **2019**, *48*, 971−988.
(42) Dorairaj, D. P.; Haribabu, J.; Mahendiran, D.; Malekshah, R. E.; Hsu, S. C. N.; Karvembu, R. Anti-proliferative potential of copper(I) acylthiourea complexes with triphenylphosphine against breast cancer cells. *Appl. Organomet. Chem.* **2023**, *37*, No. e7087.
(43) Xue, F.; Xie, C.-Z.; Zhang, Y.-W.; Qiao, Z.; Qiao, X.; Xu, J.-Y.; Yan, S.-P. Two new dicopper(II) complexes with oxamido-bridged ligand: Synthesis, crystal structures, DNA binding/cleavage and BSA binding activity. *J. Inorg. Biochem.* **2012**, *115*, 78−86.
(44) Suganthi, M.; Elango, K. P. Synthesis, characterization and serum albumin binding studies of vitamin K3 derivatives. *J. Photochem. Photobiol., B* **2017**, *166*, 126−135.
(45) Mannhold, R.; Poda, G. I.; Ostermann, C.; Tetko, I. V. Calculation of molecular lipophilicity: State-of-the-art and comparison of Log *P* methods on more than 96,000 compounds. *J. Pharm. Sci.* **2009**, *98*, 861−893.
(46) Scolaro, C.; Hartinger, C. G.; Allardyce, C. S.; Keppler, B. K.; Dyson, P. J. Hydrolysis study of the bifunctional antitumour compound RAPTA-C, [Ru(η^6-*p*-cymene)Cl_2(pta)]. *J. Inorg. Biochem.* **2008**, *102*, 1743−1748.
(47) Kamatchi, T. S.; Chitrapriya, N.; Lee, H.; Fronczek, C. F.; Fronczek, F. R.; Natarajan, K. Ruthenium(II)/(III) complexes of 4-hydroxy-pyridine-2,6-dicarboxylic acid with PPh_3/$AsPh_3$ as co-ligand: Impact of oxidation state and co-ligands on anticancer activity *in vitro*. *Dalton Trans.* **2012**, *41*, 2066−2077.
(48) Rohini, G.; Haribabu, J.; Aneesrahman, K.; Bhuvanesh, N. S. P.; Ramaiah, K.; Karvembu, R.; Sreekanth, A. Half-sandwich Ru(II)(η^6-*p*-cymene) complexes bearing *N*-dibenzosuberenyl appended thiourea for catalytic transfer hydrogenation and *in vitro* anticancer activity. *Polyhedron* **2018**, *152*, 147−154.
(49) Barolli, J. P.; Maia, P. I.; Colina-Vegas, L.; Moreira, J.; Plutin, A. M.; Mocelo, R.; Deflon, V. M.; Cominetti, M. R.; Camargo-Mathias, M. I.; Batista, A. A. Heteroleptic *tris*-chelate ruthenium(II) complexes of *N*,*N*-disubstituted-*N*′-acylthioureas: Synthesis, structural studies, cytotoxic activity and confocal microscopy studies. *Polyhedron* **2017**, *126*, 33−41.
(50) Becceneri, A. B.; Popolin, C. P.; Plutin, A. M.; Maistro, E. L.; Castellano, E. E.; Batista, A. A.; Cominetti, M. R. The *trans*-[Ru(PPh_3)$_2$(*N*,*N*-dimethyl-*N*′-thiophenylthioureato-k_2O,S)(bipy)]-PF_6 complex has pro-apoptotic effects on triple negative breast cancer cells and presents low toxicity *in vivo*. *J. Inorg. Biochem.* **2018**, *186*, 70−84.
(51) Colina-Vegas, L.; Luna-Dulcey, L.; Plutín, A. M.; Castellano, E. E.; Cominetti, M. R.; Batista, A. A. Half sandwich Ru(II)-acylthiourea complexes: DNA/HSA-binding, anti-migration and cell death in a human breast tumor cell line. *Dalton Trans.* **2017**, *46*, 12865−12875.
(52) Jeyalakshmi, K.; Haribabu, J.; Bhuvanesh, N. S. P.; Karvembu, R. Half-sandwich $RuCl_2$(η^6-*p*-cymene) core complexes containing sulfur donor aroylthiourea ligands: DNA and protein binding, DNA cleavage and cytotoxic studies. *Dalton Trans.* **2016**, *45*, 12518−12531.
(53) Jeyalakshmi, K.; Haribabu, J.; Balachandran, C.; Bhuvanesh, N. S. P.; Emi, N.; Karvembu, R. Synthesis of Ru(II)−benzene complexes containing aroylthiourea ligands, and their binding with biomolecules and *in vitro* cytotoxicity through apoptosis. *New J. Chem.* **2017**, *41*, 2672−2686.
(54) Becceneri, A. B.; Fuzer, A. M.; Plutin, A. M.; Batista, A. A.; Lelievre, S. A.; Cominetti, M. R. Three-dimensional cell culture models for metallodrug testing: induction of apoptosis and phenotypic reversion of breast cancer cells by the *trans*-[Ru(PPh_3)$_2$(*N*, *N*-dimethyl-*N*-thiophenylthioureato-k_2O,S)(bipy)]PF_6 complex. *Inorg. Chem. Front.* **2020**, *7*, 2909−2919.
(55) Kasibhatla, S.; Amarante-Mendes, G. P.; Finucane, D.; Brunner, T.; Bossy-Wetzel, E.; Green, D. R. Acridine orange/ethidium bromide (AO/EB) staining to detect apoptosis. *Cold Spring Harbor Protoc.* **2006**, *2006*, No. 4493.
(56) Doonan, F.; Cotter, T. G. Morphological assessment of apoptosis. *Methods* **2008**, *44*, 200−204.
(57) Harris, I. S.; DeNicola, G. M. The complex interplay between antioxidants and ROS in cancer. *Trends Cell Biol.* **2020**, *30*, 440−451.
(58) Perillo, B.; Di Donato, M.; Pezone, A.; Di Zazzo, E.; Giovannelli, P.; Galasso, G.; Castoria, G.; Migliaccio, A. ROS in cancer therapy: The bright side of the moon. *Exp. Mol. Med.* **2020**, *52*, 192−203.
(59) Spagnuolo, G.; D'antò, V.; Cosentino, C.; Schmalz, G.; Schweikl, H.; Rengo, S. Effect of *N*-acetyl-*L*-cysteine on ROS production and cell death caused by HEMA in human primary gingival fibroblasts. *Biomaterials* **2006**, *27*, 1803−1809.
(60) Liang, Q.; Wang, X. P.; Chen, T. S. Resveratrol protects rabbit articular chondrocyte against sodium nitroprusside-induced apoptosis *via* scavenging ROS. *Apoptosis* **2014**, *19*, 1354−1363.
(61) Chandel, N. S. Mitochondria. *Cold Spring Harbor Perspect. Biol.* **2021**, *13*, No. a040543.
(62) Pickar, A. D.; Benz, R. Transport of oppositely charged lipophilic probe ions in lipid bilayer membranes having various structures. *J. Membr. Biol.* **1978**, *44*, 353−376.
(63) Jarskog, L. F.; Gilmore, J. H. Developmental expression of Bcl-2 protein in human cortex. *Dev. Brain Res.* **2000**, *119*, 225−230.
(64) Miyashita, T.; Krajewski, S.; Krajewska, M.; Wang, H. G.; Lin, H.; Liebermann, D. A.; Hoffman, B.; Reed, J. C. Tumor suppressor p53 is a regulator of Bcl-2 and Bax gene expression *in vitro* and *in vivo*. *Oncogene* **1994**, *9*, 1799−1805.
(65) Otazo-Sánchez, E.; Ortiz-del-Toro, P.; Estévez-Hernández, O.; Pérez-Marín, L.; Goicoechea, I.; Cerón Beltran, A.; Villagómez-Ibarra, J. R. Aroylthioureas: New organic ionophores for heavy metal ion selective electrodes. A nuclear magnetic resonance study. *Spectrochim. Acta, Part A* **2002**, *58*, 2281−2290.
(66) Douglass, I. B.; Dains, F. The preparation and hydrolysis of mono-and disubstituted benzoylthioureas. *J. Am. Chem. Soc.* **1934**, *56*, 1408−1409.

https://doi.org/10.1021/acs.inorgchem.3c00757
Inorg. Chem. 2023, 62, 11761−11774